ISSN: 2281-1346

UNIVERSITÀ DI PAVIA
Department of Economics and Management

DEM Working Paper Series

Market Risk, Connectedness and Turbulence: A Comparison of 21st Century Financial Crises

Daniel Felix Ahelegbey
(Boston University)
(Università di Pavia)

Paolo Giudici
(Università di Pavia)

 # 188 (05-20)

Via San Felice, 5
I-27100 Pavia

economiaweb.unipv.it

Market Risk, Connectedness and Turbulence: A Comparison of 21st Century Financial Crises

Daniel Felix Ahelegbey[a,b,*], Paolo Giudici[b]

[a] *Department of Mathematics and Statistics, Boston University, USA*
[b] *Department of Economics and Management, University of Pavia, Italy*

Abstract

We construct a network-based turbulence score that proves useful for analyzing the relationship between financial interconnectedness, and global market risk, and for identifying systemically important markets, with the highest contribution to financial turbulence. We apply our measure to study the integration among the major stock markets over the first two decades of the 21st century, particularly during the tech, sub-prime, and ongoing COVID-19 crises. The result shows that the interconnectedness of the markets amplifies initial global market risks (on average almost four times), to cause financial turbulence. We also found evidence that the United States is central to global market turbulence, followed by Brazil, France, Hong Kong, and Germany.

Keywords: Centrality, COVID-19, Density, Financial Crises, Financial Networks, VAR.

JEL: C11, C15, C51, C52, C55, C58, G01, G12

1. Introduction

The reaction of world economies to the global pandemic, caused by the widespread of the novel coronavirus (COVID-19), has reignited discussions on the fragility/resilience of the financial system to turbulent events of such magnitude. The debate has centered on whether a financial system with dense market interconnections is more vulnerable/resilient to shocks. On one hand, a considerable number of studies, beginning with Allen and Gale (2000) and Freixas et al. (2000), support the conclusion that densely connected markets are more resilient to financial turmoil. Their argument is based on the premise that higher connectedness provides an avenue for risk-sharing and diversification, thereby improving financial stability. In contrast, the works by Billio et al. (2012); Blume et al. (2013) among others, show that dense financial network creates a vulnerable system for risk propagation. While these two streams of literature provide an opposing conclusion on dense financial networks, recent studies by Haldane (2013) and Acemoglu et al. (2015) show that dense market connections may be viewed as a "robust-yet-fragile" system, in the sense that when the magnitude of shocks is within a certain range, the connections serve as shock-absorbers. Beyond a tipping point, these links act as shock-amplifying channels for a systemic meltdown.

The above debate inspires the first two research questions (RQ) of our current work: (RQ-1) does a densely interconnected market reduce or amplify the financial risks caused by

*Corresponding author

Email addresses: danielfelix.ahelegbey@unipv.it (Daniel Felix Ahelegbey), dfkahey@bu.edu (Daniel Felix Ahelegbey), paolo.giudici@unipv.it (Paolo Giudici)

shock events?; and (RQ-2) Is there a threshold level of risk beyond which financial connection channels serve as shock-amplifiers?

Another topical issue in financial contagion studies is the identification of "systemically important" financial entities. These are countries, markets or institutions whose failure affects the entire financial system. Identifying such entity is of great importance to regulators, policymakers, and researchers for the formulation of regulations. Various definitions of systemic importance have been put forth in the literature on network centrality measures (Bonacich, 1972; Faust, 1997; Freeman, 1978; Newman, 2010) and systemic risk (Avdjiev et al., 2019; Billio et al., 2012; Borgatti and Everett, 2006; Diebold and Yilmaz, 2014). To some, centrality is measured by the number of connected counterparties (degree). For others, the importance is portrayed by the location of an entity in the network (betweenness or closeness), and to some, centrality depends on the importance of an entity's counterparties (eigenvector centrality, authority, hub). While these centrality measures have proved helpful, they only focus on the network properties without the relevance of an entity's risk, except Härdle et al. (2016).

The above open issue motivates our third research question: (RQ-3) which major financial market is central to the creation of financial turbulence?

We begin by modeling the return network of the world's major stock market indices as a vector autoregression residual structural equation model (VAR-RSEM). The choice of the equities market is inspired by the fact that it is at the heart of the world's financial system, and most investors look at these markets for assets to diversify their exposures and for portfolio growth. The choice of the VAR-SEM is motivated by the necessity to model structural serial and cross-lagged dependence in multivariate financial time series, as in the VAR models of (Barigozzi and Brownlees, 2019; Basu and Michailidis, 2015; Billio et al., 2012; Diebold and Yilmaz, 2014). We extend VAR models with a network structure that is estimated via a Bayesian approach. This allows us to deal with the uncertainty in network link prediction by incorporating relevant prior information and applying model averaging, as in the works of Ahelegbey et al. (2016a,b); Carvalho et al. (2007); Carvalho and West (2007). To infer the network, we build on the Bayesian graphical VAR (BGVAR) in Ahelegbey et al. (2016a,b) by applying a sequential algorithm that samples the lag structure and, then, the contemporaneous connections. Unlike the previous algorithm that draws the network separately from their marginal posterior probabilities, the current approach is sequential and improves computational efficiency, making it scalable to high dimensional models.

We address the research questions by extending the Mahalanobis measurement of Kritzman and Li (2010) to construct a network-based financial turbulence index from the intricate interaction between the interconnections and risks. Our turbulence index has three key features. One, our index is a score of the level of disruptions in global financial markets across time. Thus, it signals the direction of financial markets and provides early warnings for investors to avoid trading in certain assets during turbulent times. Our turbulence index is in a way related to systemic risk measurements but very distinct from it. For various systemic risk measures see (Adrian and Brunnermeier, 2016; Banulescu and Dumitrescu, 2015; Billio et al., 2012; Brownlees and Engle, 2017; Diebold and Yilmaz, 2014; Huang et al., 2012; Kritzman et al., 2011). The difference, however, lies in the fact that systemic risk indices assign a score to the level of vulnerability embedded in the system, while our turbulence index measures the severity of disruptions to the system, which can be caused by internal or external shocks.

The second feature of our turbulence index is that it decomposes into a product of two indicators, namely, risk and network effect. The risk effect records the magnitude of initial global market risk, and the network effect is the degree to which interconnectedness among

markets intensifies or weakens the initial global market risks. Closely related concepts to this decomposition are the magnitude and correlation surprise in Kinlaw and Turkington (2013).

The third feature of our proposed index is that it decomposes into marginal turbulence contribution (MTC) and systemic sensitivity to individual risk (SSIR), with both measures shown to be useful when assessing the relevance of a market to financial turbulence. We define MTC as the score of each financial market's contribution to the overall turbulence index and SSIR as the responsiveness of the system to a small change in an individual market's risk.

These three features outline our contribution to answering our research questions. One, we study the evolution between our network-based turbulence index and standard network density to answer (RQ-1). Two, we monitor the risk effects to identify the threshold of global market risks beyond which dense financial connections serve as shock-amplifiers, thus, answering (RQ-2). Finally, we rank the two market indicator measures to assess the relevance of each market to financial turbulence, thus answering (RQ-3).

We apply our proposed model to study the equities market by considering the 20 major stock market indices, selected for their market capitalization, covering countries across the Americas, Asia-Pacific, and Europe. The dataset consists of daily close prices from January 2000 to March 2020. The result shows that the correlation between network density and our turbulence index is 0.5565, which indicates a positive relationship between the two indices. Thus, densely interconnected networks amplify financial risks, thereby confirming the results of Billio et al. (2012); Blume et al. (2013). From the full sample analyzed, the highest risk effect recorded was 29.2 of returns (in October 2008), followed by 22.5 of returns (in March 2020), which coincide with the global financial crisis, and the ongoing COVID-19 pandemic, respectively. The network effect during these times was 4.9 and 4.1, respectively, which suggests that market interconnections played a significant role in amplifying the initial shock events. We standardized the risk and network effect indices and applied them as a barometer to study the tipping point in financial turbulence measurement. The result shows that when risk effect is above 2.0 of returns, and the network effect is beyond the mean value of 3.9, financial connection channels serve as shock-amplifiers leading to global market disruption. The centrality analysis shows that the US market is the most influential, and small changes in its risk causes the highest financial turbulence. In terms of turbulence contribution, the US is the first, followed by Brazil, France, Hong Kong, and Germany. The result also shows that, although Brazil has a higher contribution to turbulence than France, a small change in the risk of the French market has a higher turbulence amplification than that of Brazil.

The organization of the paper is as follows. In Section 2, we introduce the VAR-RSEM model and our proposed measure of turbulence. We discuss model estimation and network selection in 3. We present a description of the data in Section 4 and report the results in Section 5. Section 6 concludes the paper with a final discussion.

2. VAR-RSEM Models and Turbulence Measures

Before discussing the VAR-RSEM models and turbulence measures, we briefly introduce the general concept of network models and centrality measures.

2.1. Network Models and Centrality Measures

A network model is a convenient representation of the relationships between a set of n statistical variables (such as market returns). It is defined by the pair (V, E), in which the set of vertices (nodes) V contains the n variables and the set of edges (links) E describes

the statistical relationships between a pair of variables. In many network applications, the links are directed edges, representing statistical dependencies between the variables. In this representation, the relationships between variables can be summarized as a zero diagonal adjacency matrix A, determined by a latent binary indicator $G_{ij} \in \{0,1\}$ that denotes the presence/absence of a link between nodes such that for $i, j = 1, \ldots, n$,

$$\begin{array}{lllll} A_{ij} = 0 & \text{if} & G_{ij} = 0 & \Longrightarrow & Y_j \not\rightarrow Y_i \\ A_{ij} \neq 0 & \text{if} & G_{ij} = 1 & \Longrightarrow & Y_j \rightarrow Y_i \end{array} \tag{1}$$

where $Y_j \not\rightarrow Y_i$ means that Y_j does not influence Y_i.

A key feature of network models in financial contagion analysis is their usefulness in summarizing how densely connected are the institutions, and to identify which units are critical (or central) to the robustness or fragility of the system. The density of a network is the number of links in the estimated network divided by the total number of possible links:

$$D^{net} = 100 \times \frac{1}{n(n-1)} \sum_i \sum_j A_{ij} \tag{2}$$

The centrality of institutions in a network is measured by assigning centrality scores to the nodes in the network. Degree is the commonest measure of centrality obtained by counting the number of counterparties connected to an institution. More formally, the in-degree of node-i, $\overleftarrow{D}_i$, and the out-degree of node-j, $\overrightarrow{D}_j$, are defined by:

$$\overleftarrow{D}_i = \sum_j A_{ij}, \qquad\qquad \overrightarrow{D}_j = \sum_i A_{ij} \tag{3}$$

where $\overleftarrow{D}_i$ ($\overrightarrow{D}_j$) counts the number of links directed towards node-i (going out of node-j).

Other metrics for criticality assessment of institutions for financial contagion are eigenvector centralities (hubs and authorities). This centrality measure computes the importance score of an institution by considering the importance of its counterparties. For example, the hub and authority centrality measures assign a score to nodes by solving the following:

$$(A^{'}A)\ h = \lambda_h h, \qquad\qquad (AA^{'})\ a = \lambda_a a, \tag{4}$$

where h and a are the hub score and authority score eigenvectors, corresponding to λ_h and λ_a, the largest eigenvalues of $A^{'}A$ and $AA^{'}$ respectively.

From a financial contagion viewpoint, nodes with the highest in-degree are liable to be influenced and those with high out-degree are "influencers". However, nodes with the highest hub measures indicate high "transmitters" of risk, while nodes with high authority values are "receivers" or risk (see Billio et al., 2012; Borgatti and Everett, 2006; Diebold and Yilmaz, 2014). The above-described measures only focus on the properties of the network without considering the relevance of institutional risks. Thus, they tend to overestimate or underestimate the criticality of institutions in financial contagion analysis. The objective of this work is to construct a network-based measure of criticality using an econometric model.

2.2. A VAR-RSEM Model

Let $Y_t = (Y_{1,t}, \ldots, Y_{n,t})$ be an n-variable vector of observed market returns at time t, where $Y_{i,t}$ is the time series of variable-i at time t. We model the dynamics of Y_t as a vector

autoregression residual structural equations model (VAR-RSEM) given by

$$Y_t = \sum_{k=1}^{p} B_k \; Y_{t-k} + R_t \tag{5}$$

$$R_t = B_0 \; R_t + \varepsilon_t \tag{6}$$

where B_k is an $n \times n$ coefficients matrix such that B_{ijk} capture the effect of Y_j on Y_i with a lag of k, R_t is a vector of reduced-form residuals, B_0 is a contemporaneous coefficients matrix such that B_{ij0} records the instantaneous effect of a shock to Y_j on Y_i, ε_t is the vector of error terms at time t that quantifies the factors that are not considered in the model, and it is assumed to be independent and identically distributed as a multivariate normal distribution with zero mean and a diagonal covariance matrix $\Sigma_\varepsilon = \text{diag}\{\sigma^2_{\varepsilon_i}\}$.

The formulation above is a variant of the general structural VAR model, a convenient framework for analyzing and forecasting out-of-sample observations of multiple time series. The objective of the model is to estimate the matrices $(B_0, B_{1:p}, \Sigma_\varepsilon)$ employing the available data. The VAR-RSEM parameters can be obtained by specifying the contemporaneous structure of the system (6) after model (5) is estimated. Model (5) is a reduced-form VAR approximation of n systems of equations with the i-th equation expressing the dependence of the i-th variable on its lag and the cross-lag effects of the remaining $n-1$ variables. Model (6) is a Residual Structural Equation Model (RSEM) representation with a system of n equations where the i-th equation represents the i-th VAR residuals expressed as a contemporaneous dependence on the remaining $n-1$ residuals. Within the VAR-RSEM formulation, the matrices B_0 and $B_{1:p}$, are of crucial importance to understand the channels of shock transmission.

2.3. A Network VAR-RSEM Model

The introduction of networks in VAR models helps to interpret the relationships in the model (Ahelegbey et al., 2016a,b; Barigozzi and Brownlees, 2019; Basu and Michailidis, 2015). For the VAR-RSEM model in (5) and (6), network nodes correspond to the observed variables. The links between the nodes correspond to significant contemporaneous or temporal dependencies, with weights measuring the estimated contemporaneous or lagged coefficients. To formalise this representation, we extend the specification of the adjacency matrix in (1) as follows. Let $G_{ijl} \in \{0, 1\}$ be a latent binary indicator that denotes the presence/absence of a link between nodes such that for $i, j = 1, \ldots, n$, and $l = 0, 1, \ldots, p$:

$$\begin{array}{lllll} B_{ijl} = 0 & \text{if} & G_{ijl} = 0 & \implies & Y_{j,t-l} \not\to Y_{i,t} \\ B_{ijl} \neq 0 & \text{if} & G_{ijl} = 1 & \implies & Y_{j,t-l} \to Y_{i,t} \end{array}$$

where $Y_{j,t-l} \not\to Y_{i,t}$ means that Y_j does not influence Y_i at lag l, including $l = 0$, which correspond to contemporaneous dependence. We then define two $n \times n$ zero diagonal adjacency matrices, A^W and A^U, whose ij-th element is given by:

$$A^W_{ij} = \begin{cases} 0, & \text{if } G_{ijl} = 0, \; \forall l \\ \sum_{l=0}^{p} B_{ijl}, & \text{if } \exists! \, l : G_{ijl} = 1 \end{cases}, \qquad A^U_{ij} = \begin{cases} 0, \text{ if } A^W_{ij} = 0 & \implies Y_j \not\to Y_i \\ 1, \text{ if } A^W_{ij} \neq 0 & \implies Y_j \to Y_i \end{cases} \tag{7}$$

where A^W is a weighted adjacency matrix, and A^U is an unweighted binary indicators matrix. A^U_{ij} in (7) specifies that any two variables, (Y_i, Y_j), are connected by a directed link from Y_j to Y_i if there exist at least one VAR-RSEM coefficient, contemporaneous or lagged, that

is significantly different from zero. The matrix A^W reports the adjacency matrix with the associated weights obtained as a sum of the estimated coefficients.

Following (5), (6) and (7), a network VAR-RSEM model is fully specified by the parameters $(p, G, B, \Sigma_\varepsilon)$ where p is the lag order; $G = \{G_0, G_{1:p}\}$ determines the network structure; $B = \{B_0, B_{1:p}\}$ specifies the coefficients associated with that structure and Σ_ε is the residual variance. Note that (G_0, B_0) represents the contemporaneous part of the model and $(G_{1:p}, B_{1:p})$ the temporal part.

The available literature on financial networks is typically focused either on structural learning or on quantitative learning. In the former case, it insists on learning G and deriving summary centrality measures, as in the work of (Battiston et al., 2012; Giudici and Spelta, 2016). In the latter case, it insists on learning B and drawing inferences from it (Billio et al., 2012; Diebold and Yilmaz, 2014). The two approaches seem not to overlap except for Ahelegbey et al. (2016a,b); Corander and Villani (2006); George et al. (2008). The proposed Network VAR-RSEM models follow the spirit of the latter.

In the next section, we introduce the model estimation framework necessary to estimate all parameters of a network VAR-RSEM model. Before doing so, we introduce a set of network summary measures that are interpretable from a financial viewpoint and that can thus be employed to answer our research questions.

2.4. Network-Based Turbulence Measures

We begin by presenting the Mahalanobis turbulence measure proposed in Kritzman and Li (2010), which has been shown to provide a good representation of financial risks during periods of market turmoil. The measure constructed by the authors can be expressed as:

$$d_t \;=\; (Y_t - \mu)'\Sigma_Y^{-1}(Y_t - \mu) \;=\; \mathrm{tr}(\Sigma_Y^{-1} S_t) \tag{8}$$

where d_t indicates the turbulence measure at time t, Y_t is a $n \times 1$ vector of returns, μ is a $n \times 1$ mean returns vector, Σ_Y is the $n \times n$ covariance matrix, calculated over the whole time period, tr() is the trace operator (the sum of the diagonal elements) and $S_t = (Y_t - \mu)(Y_t - \mu)'$ is the $n \times n$ inner product matrix.

Equation (8) consists of two main components: the return partial correlations (captured by Σ_Y^{-1}) and the return standard deviations (captured by S_t). Note that, in the definition, the partial correlation matrix Σ_Y^{-1} does not have constraints on its elements. From a network perspective, this corresponds to a full adjacency matrix (that is, A^W with no off-diagonal zeros elements). We propose to replace the full adjacency matrix with a constrained one that can be obtained from the estimated A^W. Thus, we extend the Mahalanobis turbulence measure, without loss of generality and reference to a specific time point.

Proposition 1. *Consider n return variables $Y = (Y_1, \ldots, Y_n)$, with standard deviations $\sigma(Y) = (\sigma_1, \ldots, \sigma_n)$. Assume the inner-product $S_\sigma = \sigma(Y)\sigma(Y)'$ describes the risks of the returns, and $\Omega = (I + A^W)'(I + A^W)$ is their constrained partial correlations matrix. A systemic turbulence measure (T^{sys}) can then be obtained replacing in (8) Σ_Y^{-1} with Ω:*

$$T^{sys} \;=\; \frac{1}{n} tr(\Omega S_\sigma) \;=\; \frac{1}{n}\sum_i \Psi_{ii} \tag{9}$$

where $\Psi = \Omega S_\sigma$. From (9) note that the turbulence score decomposes in two main components. The matrix S_σ has individual variances on the main diagonal and products of pairs of

standard deviations on the off-diagonal.

To better understand the structure of these two matrices, consider an $n = 3$-dimensional vector (i, j, k) with standard deviations $\sigma(Y) = (\sigma_i, \sigma_j, \sigma_k)$. We then have:

$$I + A^W = \begin{pmatrix} 1 & a_{ij} & a_{ik} \\ a_{ji} & 1 & a_{jk} \\ a_{ki} & a_{kj} & 1 \end{pmatrix}, \qquad S_\sigma = \begin{pmatrix} \sigma_i^2 & \sigma_i\sigma_j & \sigma_i\sigma_k \\ \sigma_j\sigma_i & \sigma_j^2 & \sigma_j\sigma_k \\ \sigma_k\sigma_i & \sigma_k\sigma_j & \sigma_k^2 \end{pmatrix}$$

$$\Omega = \begin{pmatrix} 1 + a_{ji}^2 + a_{ki}^2 & a_{ij} + a_{ji} + a_{ki}a_{kj} & a_{ik} + a_{ji}a_{jk} + a_{ki} \\ a_{ij} + a_{ji} + a_{kj}a_{ki} & a_{ij}^2 + 1 + a_{kj}^2 & a_{ij}a_{ik} + a_{jk} + a_{kj} \\ a_{ik} + a_{jk}a_{ji} + a_{ki} & a_{ik}a_{ij} + a_{jk} + a_{kj} & a_{ik}^2 + a_{jk}^2 + 1 \end{pmatrix}$$

where $\Omega_{ij} = (a_{ij} + a_{ji} + a_{ki}a_{kj})$ is the weight of the undirected link between i and j. Note that $\Omega_{ij} = 0$ if and only if i and j are not directly related ($a_{ij} = a_{ji} = 0$) and both variables are not related through k (i.e either $a_{ki} = 0$ or $a_{kj} = 0$). In network terminology, $a_{ki} \neq 0$ means that k is a child of i, and $a_{kj} \neq 0$ means that k is a child of j. Thus, if k is a child of both i and j, then i and j are both parents of k. So even though i and j may not be directly related ($a_{ij} = a_{ji} = 0$), they may be conditionally related through k if $a_{ki} \neq 0$ and $a_{kj} \neq 0$. The systemic turbulence, $T^{sys} = \frac{1}{n}\text{tr}\,(\Omega S_\sigma)$ is then computed as

$$\begin{aligned} T^{sys} &= \frac{1}{n}\text{tr}\left[\begin{pmatrix} \Omega_{ii} & \Omega_{ij} & \Omega_{ik} \\ \Omega_{ji} & \Omega_{jj} & \Omega_{jk} \\ \Omega_{ki} & \Omega_{kj} & \Omega_{kk} \end{pmatrix}\begin{pmatrix} \sigma_i^2 & \sigma_i\sigma_j & \sigma_i\sigma_k \\ \sigma_j\sigma_i & \sigma_j^2 & \sigma_j\sigma_k \\ \sigma_k\sigma_i & \sigma_k\sigma_j & \sigma_k^2 \end{pmatrix}\right] \\ &= \frac{1}{n}\Big[\Omega_{ii}\sigma_i^2 + \Omega_{jj}\sigma_j^2 + \Omega_{kk}\sigma_k^2 + 2\Omega_{ij}\sigma_i\sigma_j + 2\Omega_{ik}\sigma_i\sigma_k + 2\Omega_{jk}\sigma_j\sigma_k\Big] \end{aligned} \tag{10}$$

In this application, we study the evolution between our systemic turbulence index in (9) and standard network density in (2) to answer the first research question (RQ-1).

An important feature of our turbulence index is that it decomposes into two further useful measures, namely, risk (Proposition 2) and network effect (Proposition 3).

Proposition 2. *From (9), a risk effect measure (R^{sys}) can be obtained as:*

$$R^{sys} = \frac{1}{n}tr(S_\sigma) = \frac{1}{n}\sum_{i=1}^{n}\sigma_i^2. \tag{11}$$

Note that R^{sys} can be viewed as the initial global market risk computed by averaging the risks of different markets from the turbulence score in (9) when all off-diagonal elements in A^W are set to zero. We remark that the R^{sys} measure is a variant of the magnitude surprise of Kinlaw and Turkington (2013).

Proposition 3. *From (9), a network effect measure (N^{sys}) can be obtained as:*

$$N^{sys} = \frac{T^{sys}}{R^{sys}} = \frac{tr\,(\Omega S_\sigma)}{tr\,(S_\sigma)}. \tag{12}$$

Note that N^{sys} measures the degree to which interconnectedness intensifies or weakens initial global market risks. The network effect can also be linked to the correlation surprise in Kinlaw and Turkington (2013). Thus, it isolates the effect of interconnectedness in the turbulence

score. Clearly, the network intensifies the initial risks when $N^{sys} > 1$, and weakens it with $N^{sys} < 1$.

Corollary 1. *From Proposition 3, the systemic turbulence score decomposes into:*

$$T^{sys} = N^{sys} R^{sys} \tag{13}$$

where R^{sys} expresses initial market risks and N^{sys} is how such risks are "amplified" in the system through interconnectedness.

In this study, we monitor the risk effects to identify the threshold of global market risks beyond which dense financial connections serve as shock-amplifiers, and thus, answering our second research question (RQ-2).

Another vital feature of the turbulence index in (9) is that it decomposes into marginal turbulence contribution (MTC: Proposition 4) and systemic sensitivity to individual risk (SSIR: Proposition 5), with both measures shown to be useful when assessing the relevance of an institution to financial turbulence. We define MTC as the score of each institution's contribution to the overall turbulence index, and SSIR as the responsiveness of the system to a small change in an institution's risk. See the following propositions for details.

Proposition 4. *The marginal turbulence contribution of institution-i (denoted by M_i^{sys}) is the difference between T^{sys} and T_{-i}^{sys} (the turbulence calculated without i), given by:*

$$M_i^{sys} \;=\; \frac{1}{n}\Psi_{ii} \;\approxeq\; T^{sys} - T_{-i}^{sys} \tag{14}$$

Proof. To establish the above relationship, we begin with the right-hand-side (RHS)

$$T^{sys} - T_{-i}^{sys} \;=\; T^{sys} - \frac{1}{n}\text{tr}\left[\begin{pmatrix}\Omega_{jj} & \Omega_{jk}\\ \Omega_{kj} & \Omega_{kk}\end{pmatrix}\begin{pmatrix}\sigma_j^2 & \sigma_j\sigma_k\\ \sigma_k\sigma_j & \sigma_k^2\end{pmatrix}\right] = \Omega_{[i,:][:,i]}S_\sigma \tag{15}$$

where $\Omega_{[i,:][:,i]}$ is the i-th row and column of Ω and zeros elsewhere. Thus,

$$\begin{aligned} T^{sys} - T_{-i}^{sys} \;&=\; \frac{1}{n}\text{tr}\left(\Omega_{[i,:][:,i]}S_\sigma\right) = \frac{1}{n}\text{tr}\left[\begin{pmatrix}\Omega_{ii} & \Omega_{ij} & \Omega_{ik}\\ \Omega_{ji} & 0 & 0\\ \Omega_{ki} & 0 & 0\end{pmatrix}\begin{pmatrix}\sigma_i^2 & \sigma_i\sigma_j & \sigma_i\sigma_k\\ \sigma_j\sigma_i & \sigma_j^2 & \sigma_j\sigma_k\\ \sigma_k\sigma_i & \sigma_k\sigma_j & \sigma_k^2\end{pmatrix}\right] \\ &=\; \frac{1}{n}\left[(\Omega_{ii}\sigma_i^2 + \Omega_{ij}\sigma_j\sigma_i + \Omega_{ik}\sigma_k\sigma_i) \;+\; \Omega_{ji}\sigma_i\sigma_j \;+\; \Omega_{ki}\sigma_i\sigma_k\right] \end{aligned} \tag{16}$$

where $\Omega_{ij} = \Omega_{ji}$ and $\Omega_{ik} = \Omega_{ki}$ due to the symmetry of Ω.

It is expected that the turbulence index must equal the sum of all institution's contribution to the overall index. However, in general and according to the expression in (10) and (16), $T^{sys} \neq \sum_i (T^{sys} - T_{-i}^{sys})$. This is due to the fact that the terms $\Omega_{ji}\sigma_i\sigma_j$ and $\Omega_{ki}\sigma_i\sigma_k$ are double counted. To achieve equality, the common approach is to introduce a matrix, Θ, with unit diagonal elements ($\theta_{ii} = 1$) and whose off-diagonals are such that ($\theta_{ij} + \theta_{ji} = 1$) (see Li et al., 2013, for details). The matrix Θ is used to transform $\Omega_{[i,:][:,i]}$ through the following

$$\tilde{\Omega}_{[i,:][:,i]} = \Omega_{[i,:][:,i]} \circ \Theta = \left[\begin{pmatrix}\Omega_{ii} & \Omega_{ij} & \Omega_{ik}\\ \Omega_{ji} & 0 & 0\\ \Omega_{ki} & 0 & 0\end{pmatrix} \circ \begin{pmatrix}1 & \theta_{ij} & \theta_{ik}\\ \theta_{ji} & 1 & \theta_{jk}\\ \theta_{ki} & \theta_{kj} & 1\end{pmatrix}\right] \tag{17}$$

where $(\circ)$ is the element-by-element Hadamard product. A simple choice for $\theta_{ij} = \theta_{ji} = 0.5$. Through the above transformation, the RHS expression of (14) can be obtained as

$$\begin{aligned} T^{sys} - T^{sys}_{-i} &= \frac{1}{n}\text{tr}\left(\tilde{\Omega}_{[i,:][:,i]} S_\sigma\right) = \frac{1}{n}\text{tr}\left[\begin{pmatrix} \Omega_{ii} & \theta_{ij}\Omega_{ij} & \theta_{ik}\Omega_{ik} \\ \theta_{ji}\Omega_{ji} & 0 & 0 \\ \theta_{ki}\Omega_{ki} & 0 & 0 \end{pmatrix}\begin{pmatrix} \sigma_i^2 & \sigma_i\sigma_j & \sigma_i\sigma_k \\ \sigma_j\sigma_i & \sigma_j^2 & \sigma_j\sigma_k \\ \sigma_k\sigma_i & \sigma_k\sigma_j & \sigma_k^2 \end{pmatrix}\right] \\ &= \frac{1}{n}\left[(\Omega_{ii}\sigma_i^2 + \theta_{ij}\Omega_{ij}\sigma_j\sigma_i + \theta_{ik}\Omega_{ik}\sigma_k\sigma_i) \;+\; \theta_{ji}\Omega_{ji}\sigma_i\sigma_j \;+\; \theta_{ki}\Omega_{ki}\sigma_i\sigma_k\right] \\ &= \frac{1}{n}\left[\Omega_{ii}\sigma_i^2 + \Omega_{ij}\sigma_j\sigma_i + \Omega_{ik}\sigma_k\sigma_i\right] \end{aligned} \tag{18}$$

We now consider the left-hand-side (LHS) of (14). Let $\Psi = (\Omega S_\sigma)$ and denote with $\Omega_{[i,:]}$ the i-th row of Ω and zeros elsewhere. The i-th diagonal element of Ψ is given by

$$\begin{aligned} \Psi_{ii} &= \text{tr}\left(\Omega_{[i,:]} S_\sigma\right) = \text{tr}\left[\begin{pmatrix} \Omega_{ii} & \Omega_{ij} & \Omega_{ik} \\ 0 & 0 & 0 \\ 0 & 0 & 0 \end{pmatrix}\begin{pmatrix} \sigma_i^2 & \sigma_i\sigma_j & \sigma_i\sigma_k \\ \sigma_j\sigma_i & \sigma_j^2 & \sigma_j\sigma_k \\ \sigma_k\sigma_i & \sigma_k\sigma_j & \sigma_k^2 \end{pmatrix}\right] \\ &= \Omega_{ii}\sigma_i^2 + \Omega_{ij}\sigma_j\sigma_i + \Omega_{ik}\sigma_k\sigma_i \end{aligned} \tag{19}$$

From the expressions in (18) and (19), we can establish the following equality

$$T^{sys} - T^{sys}_{-i} \;=\; \frac{1}{n}\Psi_{ii} \;=\; M_i^{sys} \tag{20}$$

□

Proposition 5. *The systemic sensitivity to risk of institution-i (denoted by S_i^{sys}) is the partial derivative of T^{sys} with respect to i's standard deviation:*

$$S_i^{sys} = \frac{\partial T^{sys}}{\partial \sigma_i} = \frac{2}{n}\Omega_{[i,:]}\sigma(Y) \tag{21}$$

where $\Omega_{[i,:]}$ is the i-th row of Ω.

Proof. Recall from (10) that

$$\begin{aligned} T^{sys} &= \frac{1}{n}\left[\Omega_{ii}\sigma_i^2 + \Omega_{jj}\sigma_j^2 + \Omega_{kk}\sigma_k^2 + 2\Omega_{ij}\sigma_i\sigma_j + 2\Omega_{ik}\sigma_i\sigma_k + 2\Omega_{jk}\sigma_j\sigma_k\right] \\ \frac{\partial T^{sys}}{\partial \sigma_i} &= \frac{1}{n}\left[2\Omega_{ii}\sigma_i + 2\Omega_{ij}\sigma_j + 2\Omega_{ik}\sigma_k\right] \;=\; \frac{2}{n}\Omega_{[i,:]}\sigma(Y) \end{aligned} \tag{22}$$

where $\Omega_{[i,:]}$ the i-th row of Ω. □

The sensitivity to individual risk and the marginal turbulence contribution are clearly related to each other. It can be shown that:

Corollary 2. *From Propositions 4 and 5, the following can be established:*

$$S_i^{sys} = \frac{2}{\sigma_i} M_i^{sys} \tag{23}$$

From the the marginal contribution to turbulence expression in (18) and (19),

$$\begin{aligned} M_i^{sys} &= \frac{1}{n}\left[\Omega_{ii}\sigma_i^2 + \Omega_{ij}\sigma_j\sigma_i + \Omega_{ik}\sigma_k\sigma_i\right] \\ &= \frac{1}{n}\sigma_i\left[\Omega_{ii}\sigma_i + \Omega_{ij}\sigma_j + \Omega_{ik}\sigma_k\right] = \frac{1}{2}\sigma_i S_i^{sys} \end{aligned} \tag{24}$$

Corollary 2 can be employed to decompose the turbulence score as a sum of local products between individual risks and sensitivities to that risk.

Corollary 3. *From Propositions 1 and 4 and corollary 2, we have the following*

$$T^{sys} = \sum_i M_i^{sys} = \frac{1}{2}\sum_i S_i^{sys}\sigma_i \tag{25}$$

The decomposition of the turbulence score (T^{sys}) into institutional level indicators (M_i^{sys} and S_i^{sys}) enables us to analyze the role of each institution in the creation of financial turbulence, thus answering our third and final research question (RQ-3).

2.5. Network Visualization

For any n-dimensional vector, we can interpret Ω (defined in Proposition 1) as symmetrized version of the weighted adjacency matrix A^W. Following Hoff (2008), we can obtain the position of nodes in network associated with A^W via an eigen-decomposition of Ω, whose ij-th entry can be parametrized as:

$$\Omega_{ij} = (C\Lambda C')_{ij} \tag{26}$$

where Ω_{ij} is the i-th row and the j-th column of Ω, $\Lambda = \text{diag}(\lambda_1, \ldots, \lambda_r)$, is a diagonal matrix of eigenvalues, C is a $n \times r$ coordinate matrix of n points in an r-dimensional system such that $C_{i,:}$ denotes the i-th row of C (that is, the coordinates of i-th node). These coordinates can provide a spatial representation of the nodes of a financial network which can be very useful for their interpretation.

3. Model Selection and Estimation

In this section we explain how the proposed network VAR-RSEM model and, consequently, the proposed turbulence measures, can be estimated from the available data. Let $Y_t = (Y_{1,t} \ldots, Y_{n,t})$ be $n \times 1$ vector of current returns, $Z_t = (Y'_{t-1}, \ldots, Y'_{t-p})'$ is $np \times 1$ vector of past returns, and denote with $Y = (Y_1, \ldots, Y_N)$ and $Z = (Z_1, \ldots, Z_N)$, a collection of Y_t and Z_t over a fixed window of length N, each of dimension $N \times n$ and $N \times np$, respectively. Let X be a stacked collection of Y and Z, with a covariance matrix $\Sigma = cov(X)$, as follows:

$$X = \begin{pmatrix} Y' \\ Z' \end{pmatrix}, \qquad \Sigma = \begin{pmatrix} \Sigma_{yy} & \Sigma_{yz} \\ \Sigma_{zy} & \Sigma_{zz} \end{pmatrix} \tag{27}$$

where X is of dimension $m \times N$ with $m = n + np$, and Σ is a $m \times m$ cross-covariance matrix for which $\Sigma_{yy} = cov(Y)$ and $\Sigma_{yz} = cov(Y, Z)$.

We first consider the estimation of $(p, B, \Sigma_\varepsilon)$, assuming that $G = \{G_0, G_{1:p}\}$ is known. Later, we remove this assumption and consider how to learn the "optimal" structure of $G = \{G_0, G_{1:p}\}$ from the data. Given G, the rest of the parameters can be estimated as follows:

1. Determine p by estimating an unrestricted VAR model and minimizing the BIC:

$$BIC(p) \;=\; \log|\hat{\Sigma}_{y|z}(p)| + n^2 p\frac{\log M}{M}, \qquad 1 \le p \le \bar{p} \tag{28}$$

where $\hat{\Sigma}_{y|z}(p) = \Sigma_{yy} - \Sigma_{yz}\Sigma_{zz}^{-1}\Sigma_{yz}'$, $M = N - p$ is the number of observations, $|\hat{\Sigma}_{y|z}(p)|$ is the determinant of $\hat{\Sigma}_{y|z}(p)$ and $\bar{p}$ is the maximum possible number of lags.

2. Estimate the coefficients of the reduced-form VAR in (5) via a Bayesian estimator, using $G_{1:p}$ as a variable selection matrix. The i-th row of $\hat{B}_{1:p}$ is given by

$$\hat{B}_{i\pi_i|1:p} = (Z_{\pi_i}'Z_{\pi_i} + \eta I_d)^{-1}Z_{\pi_i}'Y_i \tag{29}$$

where $Z_{\pi_i} \in Z$ are the lag predictors of Y_i, I_d denotes an d-dimensional identity matrix with d the number of covariates in Z_{π_i} and η is a hyper-parameter which gives the prior precision of the coefficients.

3. Estimate the covariance matrix in the SEM model in (6) as:

$$\hat{R}' = Y' - \hat{B}_{1:p}Z', \qquad \text{and} \qquad \hat{\Sigma}_R = cov(\hat{R}) \tag{30}$$

4. Use G_0 as a variable selection matrix to estimate $\hat{B}_0$ - the coefficients of the residual SEM, and the covariance matrix $\hat{\Sigma}_\varepsilon$ of structural errors. The i-th row of $\hat{B}_0$ is given by

$$\hat{B}_{i\pi_i|0} = (\hat{R}_{\pi_i}'\hat{R}_{\pi_i} + \eta I_d)^{-1}\hat{R}_{\pi_i}'\hat{R}_i, \qquad \text{and} \qquad \hat{\Sigma}_\varepsilon = (I - \hat{B}_0)\hat{\Sigma}_R(I - \hat{B}_0)' \tag{31}$$

where $\hat{R}_{\pi_i} \in \hat{R}_{-i} = \hat{R}\backslash\{\hat{R}_i\}$ is the restricted set of contemporaneous predictors of the i-th equation of the residual SEM model whose dependent variable is $\hat{R}_i$.

What is described so far is conditional on a given structure for G. Estimating G is crucial for deciding which elements of $B_{1:p}$ and B_0 should be included or excluded in the final model. While the estimation process of $(p, B, \Sigma_\varepsilon)$ is an adaption of methods known in the literature, for the estimation of G, we propose a Bayesian graphical VAR (BGVAR) approach. The approach is based on a search-and-score technique that explores all networks within the space of possible configurations, assigns a score to each of them, and, finally, averages the link probability across the models with the highest scores. More precisely, the proposed BGVAR is made up of three main building blocks:

(i) A network score function
(ii) A network search algorithm
(iii) A link probability model

We now describe each of the above-mentioned components.

3.1. Network Score Function

Let U and W be two random variables and let $\mathcal{D}$ be the available data. Consider U and W, a dependent and explanatory variable respectively. The network matrix $G_{uw} = 1$ establishes the relationship $W \to U$, and the score function assigns a score to this relationship. Following Geiger and Heckerman (2002), the closed-form expression for Score$(G_{uw} = 1) = \log P(W \to$

$U|\mathcal{D}) = \log P(U|W,\mathcal{D})$ equal to:

$$P(U|W,\mathcal{D}) = \frac{\pi^{-\frac{1}{2}N}\ \nu_0^{\frac{1}{2}\nu_0}}{\nu_n^{\frac{1}{2}\nu_n}} \frac{\Gamma\left(\frac{\nu_0+N-n_f}{2}\right)}{\Gamma\left(\frac{\nu_0-n_f}{2}\right)} \left(\frac{|\bar{\Sigma}_{ww}|}{|\bar{\Sigma}_{ff}|}\right)^{\frac{1}{2}\nu_n}, \tag{32}$$

where $f = (u \cup w)$ is the union of the indexes of U and W, $n_f = |f|$ is the number of elements in f, $\nu_0 > m$ is a degree of freedom hyper-parameter of the prior precision of Σ, $\nu_n = \nu_0 + M$, $\bar{\Sigma}_{ww}$ and $\bar{\Sigma}_{ff}$ are the posterior covariance matrices of $\{W\}$ and $\{(U,W)\}$. As shown, for example, in Geiger and Heckerman (2002), the latter can be obtained from the full posterior distribution of Σ given by

$$\bar{\Sigma} = \frac{1}{\nu_n}(X'X + \nu_0 I_m), \tag{33}$$

where I_m is an m-dimensional identity matrix with m the number of variables in X.

A careful look at (32) indicates that only the ratio of the posterior covariances depends on the data. Thus, for computational efficiency, we can pre-compute the part of the score function that is independent of the data, for different values of $n_f \in [1, np+1]$ and for fixed $\nu_0 = m+2$ and N. In addition, we can pre-compute the posterior of the full covariance matrix according to (33), and save computational time by extracting the sub-matrices $\bar{\Sigma}_{ww}$ and $\bar{\Sigma}_{ff}$ of the indexes that corresponds to $\{W\}$ and $\{(U,W)\}$. This is in line with the local computation approach introduced by (Dawid and Lauritzen, 1993; Geiger and Heckerman, 2002; Giudici and Green, 1999; Grzegorczyk and Husmeier, 2008).

3.2. Network Search Algorithm

Following the expression in (32), letting $U = Y_i$, the next step of BGVAR inference is to find the combination of variables in $W = W_{yz} \in (Y_{-i}, Z)$ that maximizes the score function, with $Y_{-i} = Y \backslash \{Y_i\}$. In other words, the objective of the network search algorithm is to sample a combination of vertices $W_{yz} \in (Y_{-i}, Z)$ that can help to predict Y_i. Since our overall VAR-RSEM model is constructed to estimate the VAR, followed by RSEM, we incorporate the same idea into the search algorithm. Following Ahelegbey et al. (2016a), we implement a modified version of the collapsed Gibbs sampler put forward by the authors. The difference between the algorithm presented in this paper and that of the authors is that the current version is implemented sequentially rather than independently. More precisely, the algorithm is designed to the first search for the combination of vertices $W_z \in Z$ that most likely generates $G_{1:p}$, and then, conditionally on this (and not independently) search for $W_y|W_z \in (Y_{-i}, Z)$ that most likely generate G_0. Correspondingly, the Gibbs sampler simulation aimed at estimating the posterior graph structure probabilities iterates as follows:

1. Sample the lag network, $[G_{1:p}|\mathcal{D}]$ by searching for $W_z \in Z$
2. Sample the contemporaneous network, $[G_0|\mathcal{D}, G_{1:p}]$ by searching for $W_y|W_z \in (Y_{-i}, Z)$

In the following, we present these two steps in more detail.

3.2.1. Sampling Lag Network

We initialize the search by first computing the conditional probability of Y_i given each $Z_j \in Z$, i.e $P(Y_i|Z_j,\mathcal{D})$, and comparing it with a reference score of the marginal probability of Y_i, $P(Y_i|\mathcal{D})$. If $P(Y_i|Z_j,\mathcal{D}) > P(Y_i|\mathcal{D})$, then Z_j contain reliable information to improve the

prediction of Y_i, thus, Z_j is a candidate lag predictor of Y_i. This allows us to have a subset $W_z \in Z$ of lag variables to consider for learning the combination that produces the highest score. Although we begin the search with this subset of variables, we also allow for other candidates in Z that may not have been selected but which can improve the explanatory power of the network model. The algorithm explores a considerable number of combination of lag predictors and applies model averaging over networks with different configurations in the highest score regions. The final result of model averaging produces a highly representative network structure. A detailed description of how to sample $G_{1:p}$ is presented in Appendix A.1.

3.2.2. Sampling Contemporaneous Network

Here our focus is on the contemporaneous network, looking for the best combination of predictors for each dependent variable. Given the optimal lag predictors from the $G_{1:p}$ sampling step, the second step of the algorithm investigates if the random addition of any of the variables in Y_{-i} can improve the explanatory power of the network model. Let $W_z \in Z$ be the optimal predictors of the lag network model. If $P(Y_i|Y_j, W_z, \mathcal{D}) > P(Y_i|W_z, \mathcal{D})$ for $Y_j \in Y_{-i}$, Y_j is a candidate contemporaneous predictor of Y_i which, if combined with $W_z \in Z$ can improve the network model performance. We then proceed by searching for possible combinations of $W_y \in Y_{-i}$ such that $W_y|W_z \in (Y_{-i}, Z)$ improves the explanatory power of the network model. We then finish off with model averaging to obtain a more appropriate network structure. A detailed description of how to sample G_0 is presented in Appendix A.2.

3.3. Network Link Probability Model

We monitor the Gibbs sampling MCMC algorithm to ensure the convergence of the chain and to construct a criterion to identify significant links. We monitor the mixing of the MCMC using the sampled network scores at each iteration to compute the potential scale reduction factor (PSRF) of Gelman and Rubin (1992). The criterion is such that if PSRF ≤ 1.2 the chains have converged. In this application, we ensure that this condition is satisfied.

We then proceed to compute marginal edge posterior probabilities by model averaging over the sampled networks. Let $\hat{\gamma}_{ij}$ be the average of the ij-th entry over the sampled networks. Using the credibility criterion in Ahelegbey et al. (2016a), we can parametrize the ij-th entry of the estimated network $\hat{G}$ with the link function:

$$\hat{G}_{ij} = \mathbf{1}(\xi_{ij} > \tau), \qquad \xi_{ij} = \hat{\gamma}_{ij} - z_{(1-\alpha)}\sqrt{\frac{\hat{\gamma}_{ij}(1-\hat{\gamma}_{ij})}{n_{\text{eff}}}}, \qquad n_{eff} = \frac{H}{1 + 2\sum_{t=1}^{\infty}\rho_t} \tag{34}$$

where n_{eff} is the Markov chain effective sample size (see Casella and Robert, 2004, pp. 499-500) representing the number of independent posterior samples of the graph, H is the total number of posterior samples of the graph, ρ_t is the autocorrelation of the graph scores at lag t, and $z_{(1-\alpha)}$ is the z-score of the normal distribution at $(1-\alpha)$ significance level. A default value for τ is 0.5, α is 0.05 and $z_{(1-\alpha)} = 1.65$.

4. Data Description

The data we consider to illustrate our methodology is taken from the Bloomberg database and consists of the daily market indices of 20 countries, selected according to their market capitalization. We consider only one index per country, which typically contains the stock prices of the largest companies listed in the nation's largest stock exchange. The considered

countries can be grouped into three regions: the Americas (Brazil, Canada, Mexico, and the United States), Asia-Pacific (Australia, China, Hong Kong, India, Japan and South Korea), and Europe (Belgium, France, Germany, Italy, the Netherlands, Portugal, Russia, Spain, Switzerland, and the United Kingdom). A description of the market indices chosen for the selected countries is presented in Table 1. The data cover January 3, 2000 to March 31, 2020. The selected market indices vary in terms of composition, in the sense that some have

Region	No.	Country	Code	Description	Index
Americas	1	Brazil	BR	Brazil Bovespa	IBOV
	2	Canada	CA	Canada TSX Comp.	SPTSX
	3	Mexico	MX	Mexico IPC	MEXBOL
	4	United States	US	United States S&P 500	SPX
Asia-Pacific	5	Australia	AU	Australia ASX 200	AS51
	6	China	CN	China SSE Comp.	SHCOMP
	7	Hong Kong	HK	Hong Kong Hang Seng	HSI
	8	India	IN	India BSE Sensex	SENSEX
	9	Japan	JP	Japan Nikkei 225	NKY
	10	Korea	KR	South Korean KOSPI	KOSPI
Europe	11	Belgium	BE	Belgium BEL 20	BEL20
	12	France	FR	France CAC 40	CAC
	13	Germany	DE	Germany DAX 30	DAX
	14	Italy	IT	Italy FTSE MIB	FTSEMIB
	15	Netherlands	NL	Netherlands AEX	AEX
	16	Portugal	PT	Portugal PSI 20	PSI20
	17	Russia	RU	Russia MOEX	IMOEX
	18	Spain	ES	Spain IBEX 35	IBEX
	19	Switzerland	CH	Switzerland SMI	SMI
	20	United Kingdom	UK	UK FTSE 100	UKX

Table 1: Detailed description of stock market indices of countries classified according to regions.

a smaller number of stocks compared to others. For instance, the U.S. is represented by the S&P 500, which contains the stocks of the top 500 large-cap corporations, whereas France is represented by CAC 40, which contains 40 stocks selected among the top 100 corporations.

Figure 1 reports the time series plot of the daily index closing prices, on a logarithmic scale. Due to differences in the values, plotting the original prices would be difficult to visualize. We, therefore, scale the prices to a zero mean and unit variance and add the absolute minimum value of each series to avoid negative outcomes. This standardizes the scale of measurement for the different series. Panel A of the figure reports the national indices, while Panel B shows a comparison between the scaled values for the United States market, as a benchmark, and the averaged scaled values for Asia-Pacific and Europe. We also report, separately, a global index constructed as the average of all 20 series. Figure 1 clearly shows that, amid many fluctuations, and some local specificities, stock market indices are highly synchronized and have been affected by three major downturns, that are grey-shaded in the Panel B of Figure 1: 2000–2003 period (the "tech" crisis); 2007–2009 ("sub-prime" crisis); and the March 2020 (COVID-19 crisis). To help the interpretation of grey-shaded periods, Table 2 reports a summary description of the main events recorded during the major downturn periods.

The look back at historical events in Figure 1 and Table 2 shows that financial markets are initially slow to adjust to the emergence of a crisis. They, however, tend to over-react as the crises begin to spread and affect different markets, either directly or through interconnected-

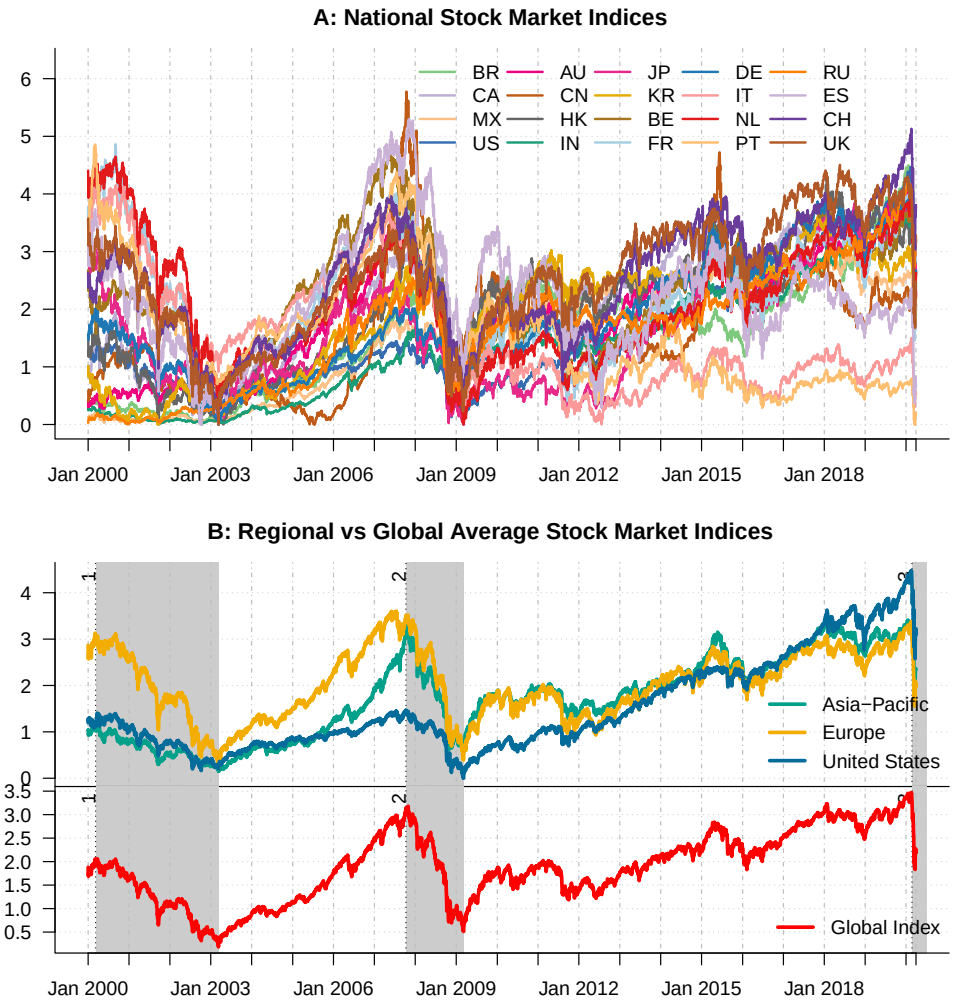

Figure 1: Time series of scaled daily national, regional, and global average stock market prices (January 3, 2000 – March 31, 2020). Gray-shadings represent periods of significant downturns in the averaged global index.

	Dates	Event Details
1	Mar 10, 2000 – Mar 12, 2003	Collapse of Dot-com bubble (Mar 10, 2000) Decline in economic activity after Sept 11, 2001 Stock market downturn of Oct 9, 2002
2	Oct 11, 2007 – Mar 9, 2009	Fall in housing prices that peaked in Oct 2007 Near-collapse and acquisition of Bear Sterns in Mar 2008 Bankruptcy of Lehman Brothers & bailout of AIG in Sep 2008
3	Feb 24, 2020 –	COVID-19 outbreak in China in late 2019 began to affect Europe and the U.S., plunging many stock markets into turmoil.

Table 2: Stock market large downturns between January 2000 – March 2020.

ness. Although there is not yet much data to fully compare the current COVID-19 crisis with the previous tech and sub-prime crisis, the daily plunge in index prices between February 24, 2020, and March 31, 2020, as illustrated in Figure 1 provides evidence that market decline occur simultaneously for all the three periods.

To better understand the peculiarity of the different crises, Table 3 presents the dates and values of the largest downturns, for each market, and across the three crisis periods. We

Country	2000 – 2003	2007 – 2009	2020
Brazil	9.63 : 2001-09-11	12.10 : 2008-10-15	**15.99** : 2020-03-12
Canada	8.47 : 2000-10-25	9.79 : 2008-12-01	**13.18** : 2020-03-12
Mexico	**8.27** : 2000-04-14	7.27 : 2008-10-22	6.64 : 2020-03-09
United States	6.00 : 2000-04-14	9.47 : 2008-10-15	**12.77** : 2020-03-16
Australia	5.55 : 2000-04-17	8.71 : 2008-10-10	**10.20** : 2020-03-16
China	6.54 : 2002-01-28	**9.26** : 2007-02-27	3.94 : 2020-01-28
Hong Kong	9.29 : 2001-09-12	**13.58** : 2008-10-27	4.98 : 2020-03-23
India	7.42 : 2000-04-04	11.60 : 2008-10-24	**14.10** : 2020-03-23
Japan	7.23 : 2000-04-17	**12.11** : 2008-10-16	6.27 : 2020-03-13
Korea	**12.80** : 2001-09-12	11.17 : 2008-10-24	8.77 : 2020-03-19
Belgium	5.61 : 2001-09-11	8.32 : 2008-09-29	**15.33** : 2020-03-12
France	7.68 : 2001-09-11	9.47 : 2008-10-06	**13.10** : 2020-03-12
Germany	8.87 : 2001-09-11	7.43 : 2008-01-21	**13.05** : 2020-03-12
Italy	7.87 : 2001-09-11	8.60 : 2008-10-06	**18.54** : 2020-03-12
Netherlands	7.53 : 2001-09-14	9.59 : 2008-10-06	**11.38** : 2020-03-12
Portugal	4.57 : 2001-09-11	**10.38** : 2008-10-06	10.27 : 2020-03-12
Russia	10.48 : 2003-10-30	**20.66** : 2008-10-06	8.65 : 2020-03-12
Spain	5.99 : 2001-09-14	9.59 : 2008-10-10	**15.15** : 2020-03-12
Switzerland	7.33 : 2001-09-11	8.11 : 2008-10-10	**10.13** : 2020-03-12
United Kingdom	5.89 : 2001-09-11	9.27 : 2008-10-10	**11.51** : 2020-03-12

Table 3: Dates of the largest daily downturn in national stock market indices during the tech crisis (2000–2003), the sub-prime crisis (2007–2009), and the recent COVID-19 crisis (2020). Bold values indicate the maximum drop of each index over the three crisis periods.

notice from the table that, during the tech crisis, the largest daily drop in the US S&P 500 was 6 percent, recorded on April 14, 2000; during the sub-prime crisis it was 9.5%, on October 15, 2008; and 12.8% on March 16, 2020 during the COVID-19 outbreak. Indeed, Table 3 suggests that, compared with other crises, the COVID-19 pandemic is having an unprecedented impact on the world's major equity markets, with 13 out of the top 20 national stock market indices recording their maximum daily downturn of the 21st century occurring in March 2020.

We compute daily returns as the log differences of successive daily closing prices, that is, $Y_{i,t} = 100\,(\log P_{i,t} - \log P_{i,t-1})$, with $P_{i,t}$ the daily closing price of market i on trading day t. Table 4 reports a set of summary statistics for the index returns over the period from January 4, 2000 to March 31, 2020. From the summary statistics, we notice that almost all index returns have a near-zero mean and a relatively high standard deviation, which ranges between 1.01 (Australia) and 1.98 (Russia). The highest standard deviations, indicating individual market volatilities, are those of the emerging markets of Russia and Brazil. The markets of Russia, Italy, and Brazil have the lowest minimum returns, while Russia, India, and Brazil have the highest maximum returns. The skewness of the returns ranges between -0.93 (Canada) and -0.04 (Mexico), indicating that all of them have distributions with mostly small but consistent positive gains and, occasionally, large negative returns, suggesting that most volatility arises from the left part of the distribution. The kurtosis varies between 5.4 (China) and 17.5 (Canada), indicating a leptokurtic behavior of the daily return series.

Country	Code	Mean	St. Dev.	Min	Max	Skew	Kurt
Brazil	BR	0.0283	1.7957	-15.9930	13.6783	-0.3971	7.0544
Canada	CA	0.0090	1.1311	-13.1758	11.2945	-0.9347	17.5301
Mexico	MX	0.0307	1.2684	-8.2673	10.4407	-0.0410	5.6344
United States	US	0.0111	1.2404	-12.7652	10.9572	-0.3825	11.5896
Australia	AU	0.0094	1.0115	-10.2030	6.7665	-0.7811	9.1395
China	CN	0.0135	1.5283	-9.2561	9.4010	-0.3207	5.4109
Hong Kong	HK	0.0059	1.4384	-13.5820	13.4068	-0.1032	8.2888
India	IN	0.0329	1.4486	-14.1017	15.9900	-0.3769	9.8492
Japan	JP	-0.0000	1.4627	-12.1110	13.2346	-0.3779	6.8760
Korea	KR	0.0103	1.4715	-12.8047	11.2844	-0.5724	7.5077
Belgium	BE	-0.0026	1.2589	-15.3275	9.3340	-0.4484	10.3656
France	FR	-0.0058	1.4412	-13.0983	10.5946	-0.2181	6.4959
Germany	DE	0.0075	1.4786	-13.0549	10.7975	-0.1753	6.0329
Italy	IT	-0.0171	1.5366	-18.5411	10.8742	-0.5943	9.3923
Netherlands	NL	-0.0065	1.4036	-11.3758	10.0283	-0.2218	7.5473
Portugal	PT	-0.0207	1.1906	-10.3792	10.1959	-0.4289	7.5186
Russia	RU	0.0543	1.9810	-20.6571	25.2261	-0.2013	16.5058
Spain	ES	-0.0104	1.4691	-15.1512	13.4836	-0.3235	8.1606
Switzerland	CH	0.0040	1.1614	-10.1339	10.7876	-0.2994	8.0790
United Kingdom	UK	-0.0039	1.1846	-11.5117	9.3843	-0.3447	8.4262

Table 4: Statistics of daily returns for stock market indices (January 4, 2000 – March 31, 2020).

5. Empirical Findings

We apply our proposed estimation methodology to obtain monthly estimates of all VAR-RSEM parameters and, in particular, of the matrices Ω and S_σ, which are the core components of our network-based turbulence score. To improve the efficiency of the estimates of Ω we aggregate monthly estimates in yearly rolling windows of about 240 trading days. We set the increments between successive rolling windows to one month, setting the first window of our study from February 1, 1999, to January 31, 2000, followed by March 1, 1999, to February 29, 2000; the last window is from April 1, 2019, to March 31, 2020. In total, we consider 243 rolling windows. To avoid over smoothing, S_σ is instead estimated monthly, that is, using only the last month of each rolling window. We present our main findings in line with answering the following research questions:

RQ-1 Does a densely interconnected market reduce or amplify the financial risks caused by shock events?

RQ-2 Is there a threshold level of risks beyond which financial connection channels serve as shock-amplifiers?

RQ-3 Which major world market is central to the creation of global financial turbulence?

We answer RQ-1 by studying the relationship between standard network density and our turbulence index (D^{net} and T^{sys} in Section 5.1). We monitor the risk and network effects (R^{sys} and N^{sys}) to identify the threshold of global market risks beyond which dense financial connections serve as shock-amplifiers, and thus, answering (RQ-2 in Section 5.2). Finally, we rank the two market indicator measures (M^{sys} and S^{sys}) to assess the relevance of each market to financial turbulence, thus answering (RQ-3 in Section 5.3).

5.1. Network Density and Financial Turbulence

Here we address our first research question: (RQ-1) Does a densely interconnected network reduce or amplify the financial risks caused by shock events?

To answer this question, we investigate the relationship between the network density and our turbulence index. Figure 2 shows the joint evolution of the two indices obtained via the described yearly moving window aggregation of the estimated parameters.

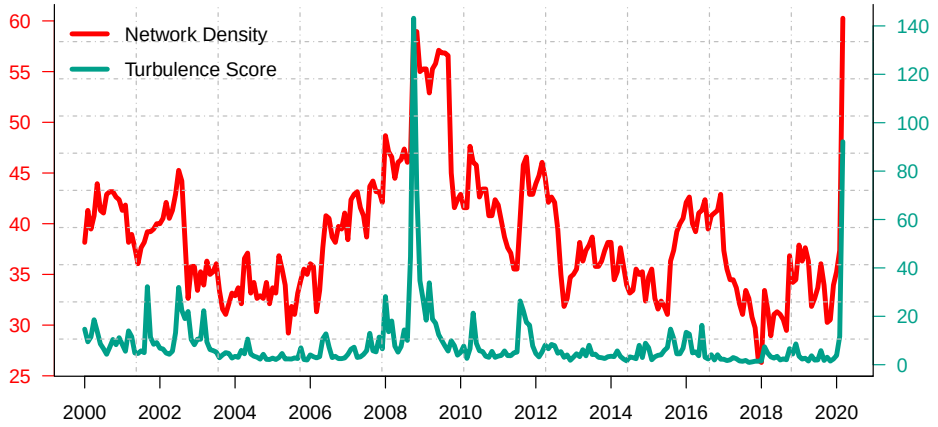

Figure 2: Network Density and Systemic Turbulence Scores from rolling windows estimation (2000-2020).

The result from the figure shows that, although the two indices have a different range of values, they have a correlation coefficient of 0.556, which indicates a positive relationship between the two measures. While the turbulence measure is highly concentrated, and reaches a strong peak in October 2008, with a value that is 143.17 standard deviations higher than the average, the network density is more disperse and shows about five peaks. Note in particular what occurs in the last point of the series, corresponding to March 2020, when the COVID-19 pandemic hits Europe and the US. The network density reaches its maximum value of 60.26 (against 58.94 in October 2008), and the turbulence piles up at 92.13 standard deviations above the average: a remarkable value, in less than one month of crisis.

To answer RQ-1, the result shows that interconnectedness does amplify financial risks, thereby confirming the results of Billio et al. (2012); Blume et al. (2013). This is evident not only from the highly positive correlation between the two series but also comparing the periods which score the highest turbulence values: the tech crisis of 2000–2003, the global financial crisis of 2007–2009, the European sovereign crisis of 2011–2012, the Chinese stock market crash of 2015, and the COVID-19 crisis in March 2020. In all these times, both the network density and turbulence index recorded values higher than their respective means.

5.2. Turning Points in Global Financial Markets

We now turn our attention to the second research question: (RQ-2) Is there a threshold level of risks beyond which financial connection channels serve as shock-amplifiers?

We address this question by studying the joint evolution of the network and risk effect (also referred to as initial global market risk) obtained via the decomposition of the turbulence index over the rolling windows estimation (see Figure 3). Before proceeding with RQ-2, we notice that Figure 3 confirms our previous conclusions. Overall, the network effect is positively correlated with the risk effect (their correlation coefficient is indeed equal to 0.31). In parallel to what Figure 2 shows, the risk effect index is highly concentrated, and peaks in October

2008, with a value of 29.20 of returns, while the network effect is more disperse, and peaks about 5 times. In each peak period, both the network and risk effect increases. Note also that periods of lows in the network effect measure (such as 2004–2005 and early 2014–2015) correspond to lows in the risk effects measure.

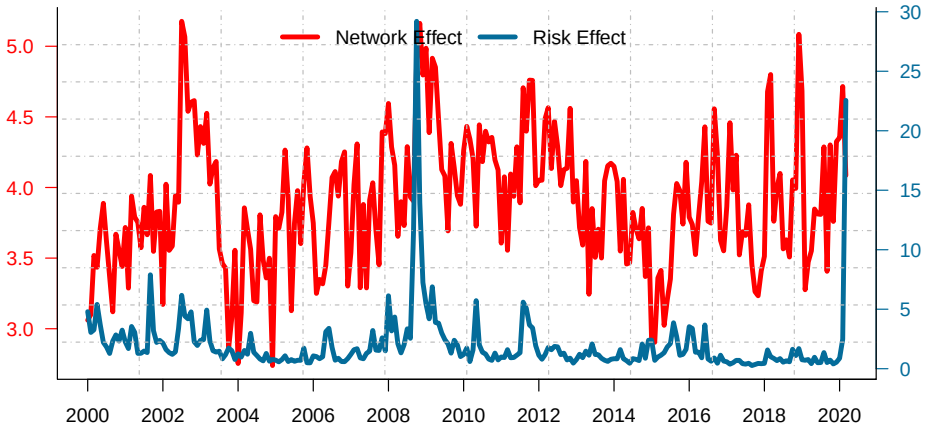

Figure 3: Network and Risk Effects obtained from the decomposition of the turbulence score.

	Min	Median	Mean	Max	St. Dev.
Network Density	26.32	37.89	38.77	60.26	58.94
Risk Effect	0.27	1.29	2.01	29.20	2.77
Network Effect	2.74	3.88	3.90	5.17	0.47
Turbulence Score	0.92	4.82	8.23	143.16	12.88

Table 5: Summary statistics of the considered network measures, with figures are rounded to the second digit.

Table 5 presents a summary statistics of the density and turbulence measures over the full sample. The statistics shows that the risk effect mimics the turbulence index, with values that range from a minimum of 0.27 (September 2017) to a maximum of 29.20 (October 2008), with a mean of 2.01 (and a median of 1.29). The network effect instead has values that range from a minimum of 2.74 (December 2004) to a maximum of 5.17 (July 2002, with 4.90 in October 2008), and a mean of 3.90 (median of 3.88). This means that the volatility generated by risk effect is amplified between 3 to 5 times by the interconnectedness. During crisis times, the risk effect peaks as well the network amplifier.

For example, during the tech crisis, a risk effect of 0.31, multiplied by a network effect of 5.17, gives mean market turbulence of 1.60 standard deviations from the mean. In the peak of the global financial crisis, the risk effect of 29.198 of returns is amplified by a network effect of 4.903 to produce a turbulence score of 143.158. This suggests an observed 20-variate return series that is 143.158 (multivariate) standard deviations from the (multivariate) mean. If we divide equally the effect among the 20 stock markets, we have that, during the financial crisis, risk effect of 1.46, amplified by a network effect of 4.90 produces a disruption of 7.15 standard deviations from its mean. A similar assessment indicates that, during the COVID pandemic in March 2020, an average risk effect of 1.12, amplified by a network effect of 4.08, yields an average turbulence score of 4.57 standard deviations from its mean. By averaging across all periods, and all 20 markets, risk effect of 0.10, multiplied by a network effect of 3.90, leads to an average turbulence score of 0.39 standard deviations from the mean.

We consider advancing the results in Table 5 by standardizing the risk and network effect indices and applying them as a barometer to classify financial market condition in each time point into "robust" and "fragile" states. To do so, we compare the monthly value of R^{sys} with its mean $E(R^{sys})$ and its standard deviation $SD(R^{sys})$ across the whole time period, to interpret its "signal" as indicating a fragile or robust market condition. More precisely, we can consider the transformation:

$$f(R_h^{sys}) = \frac{R_h^{sys} - E(R^{sys})}{SD(R^{sys})} = \begin{cases} < 0, & \Longrightarrow \text{ Robust} \\ > 0, & \Longrightarrow \text{ Fragile} \end{cases} \tag{35}$$

where $E(N^{sys})$ and $SD(N^{sys})$ is the mean and standard deviation of the risk effect. We apply a similar transformation to the network effect score.

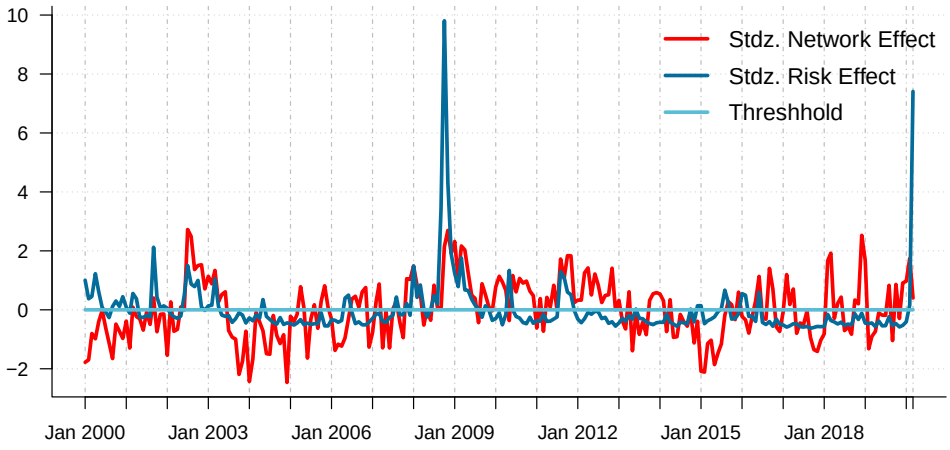

Figure 4: Standardized Network and Risk Effect.

Figure 4 presents the evolution of the standardized measures according to (35). The zero-line of the figure can be viewed as a threshold indicator for identifying turning points in global market conditions, between states of market fragility or of robustness. Note that the zero-threshold line corresponds to the mean risks and network effects reported in Table 5. When a measure is below the zero lines, it signals a "robust" market condition, and when above, it signals "fragile" conditions. From the figure, we can extract the "turning point" dates, as they emerge from the movements of the standardized network and risk effects around the zero lines. Table 6 lists the turning point dates.

Robust	Fragile	Reasons for Financial Market Fragility
-	2000:01	Collapse of Dot-com bubble
2001:05	2001:09	September 11 Effect
2002:02	2002:07	Stock market downturn of 2002
2005:05	2007:08	Sub-prime and Global Financial Crisis
2009:11	2010:05	EU Crisis - Greece debt crisis intensifies
2010:06	2011:08	EU Crisis - Crisis of Greece, Ireland & Portugal affect Spain & Italy
2011:12	2015:07	Chinese stock market turbulence
2015:10	2020:02	COVID-19 Crisis

Table 6: Identifying periods of market fragility (January 2000 – March 2020). The dates are in the format YYYY:MM and they represent the start and end of financial fragility.

The turning point dates identify the early 2000's as a period of market fragility. This is the tech (dot-com bubble) crisis, fuelled by the adoption of the internet in the late 1990s, especially in developed markets. During the early 2000's, tech-companies in these countries capitalized on high investor demands, which inflated stock price. Then, a slowdown in the United States led to investors cashing out their investment, triggering a downward movement of prices of many developed market indices around March 2000. Although this event disrupted global market operations, Figure 4 suggests that the impact of the dot-com bubble on the global market was mild compared to the other two crises that followed.

The switch to robust market conditions in May 2001 was interrupted by the impact of the event of September 11, 2000. Again the February 2002 recovery was short-lived due to the downturn in July 2002. Markets finally recovered in May 2005 until the outburst of the sub-prime crisis in August 2007. According to the financial reports, the US began to face disruptions around early- to mid-2007, due to many top institutions holding mortgage-related securities and those with high leverage crumbling under the weight of liquidity shocks following the fall in housing prices and abrupt shutdown of sub-prime lending. This, however, did not receive global attention until the losses in US sub-prime mortgages began to affect other multinational institutions around mid- to late-2007. For instance, the global impact was felt after the signal from the French BNP Paribas in August 2007 triggered the reaction of other big market players around the world. Though this disruption began late-2007, the global impact began to manifest in early 2008.

After the financial crisis, the standardized measures signal a transition to a robust market in late 2009, and a new state of fragility during the early stages of the European Sovereign crisis that began with Greece debts intensifying around May 2010. Though the effect seemed on the global market was very small, the problem resurfaced in August 2011, when the crisis of Greece, Ireland, and Portugal began to affect Spain and Italy (the third largest Euro area economy and second-biggest debtor to bond investors). This triggered new heights of the crisis with reactions across other EU member states and markets. The global market recovered in around December 2012. After which a period of robust markets follows, and was interrupted by the Chinese stock market turbulence in late 2015. The plot of the standardized risk effect in Figure 4 shows that the effects of the European sovereign and Chinese crises had a limited, or more regional, impact on global market operations.

As shown in Figure 4 and Table 6, robust market conditions that persisted between late 2015 to early 2020 have been abruptly interrupted by the COVID-19 crisis, whose effect in terms of turbulence score, risk effect, and network effect are within the range of values comparable to that of the global financial crisis, although the effect on most countries is less than one month of our sample data. The result shows that, in crisis times, both the risk effect and the network effect are strongly above the threshold line, and tightly coupled with each other. This suggests that, during crisis, risk events affecting the major stock markets can become very severe through network amplification.

In summary, the result shows an average risk and network effects of 2.0 and 3.90, respectively. Thus, when the global market risk is higher 2.0 of returns and the network effect is higher than 3.9, the multiplicative effect of interconnectedness may generate a meltdown. For instance, over the first two decades of the 21st century, the highest global market risk recorded were 29.2 of returns, followed by 22.5 at the end of October 2008 and March 2020, respectively. These occurred during the global financial crisis and the ongoing COVID-19 pandemic. The associated network effect were 4.9 and 4.1, respectively.

5.3. Network Centrality and Financial Turbulence

We now address our third research question: (RQ-3) Which major world market is central to the creation of global financial turbulence?

To address this question, we study the relationship between interconnectedness and centrality, investigating which markets are more central and, therefore, systematically more relevant to financial market turbulence over the first two decades of the 21st century.

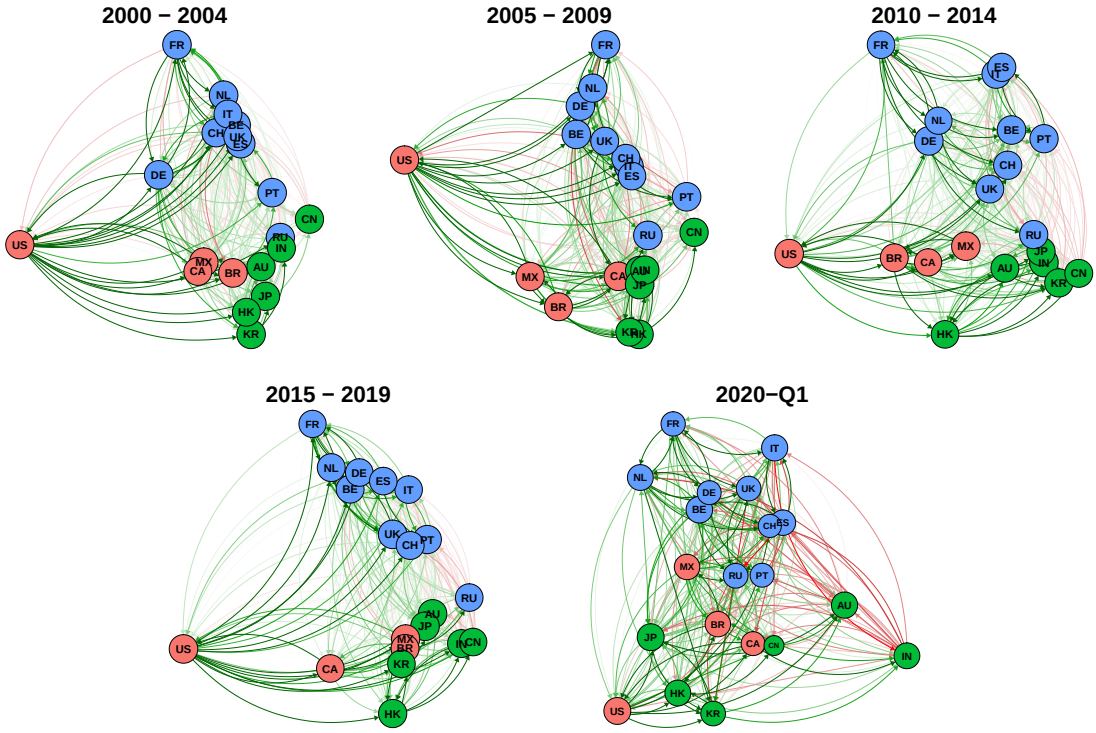

Figure 5: A representation of the network structure for the sub-windows 2000:01–2020:03. Countries are positioned based on their latent coordinates following the eigen-decomposition in (26). Red nodes denote markets in the Americas, blue for European countries, and green for Asia-Pacific countries.

We report in Figure 5 the networks for the markets by applying (26) to the estimated network structures, averaged for four consecutive periods of five years, and 2020-Q1. Each network is represented with links that are color-coded according to the sign of the relationships obtained from the Ω matrix. Positive effects are depicted with green links and negative ones are represented in red. The nodes are also color-coded according to regions, i.e., red nodes denote markets in the Americas, blue for European countries, and green for Asia-Pacific countries. The position of the countries are based on the eigen-decomposition of the networks. It reveal the tendency for markets to move together due to similarities in underlying market conditions. Thus, markets with similar characteristics are likely to be closer to each other, while those with different underlying conditions are likely to be farther apart.

From Figure 5, we notice that the positions of the markets are quite stable over time. Except for 2020-Q1, the various sub-period networks reveal three clusters of countries over time. In one cluster is the US alone, EU countries except Russia form a second cluster, and Asia-Pacific with the rest of the Americas, apart from the US, form the third cluster. The US market appears to be in a class of its own and highly linked to the rest of the world's major stock markets. The EU markets have a strong tendency to move together, with the

obvious exception of the Russian market, which is closer to Asia-Pacific markets. France is on one extreme of the European cluster, with strong links with the US, and tightly related with Northern European countries (DE, NL), and to West/Southern European countries (BE, ES, IT, PT). To the other extreme, the UK and Switzerland are well connected with both American and Asia-Pacific markets. A similar clustering pattern occurs for the Asia-Pacific markets, although to a lesser extent. The rest of the Americas (without the US) appear more aligned to the Asia-Pacific cluster. Although there is still evidence of the clustering pattern in the 2020-Q1 network, especially among the EU countries, that of the Americas and Asia-Pacific are quite scattered, reflecting the heterogeneity of the underlying markets.

5.3.1. Full-Sample Systemic Relevance

To specifically address RQ-3, we report in Table 7, the full sample median summary statistics of the marginal turbulence contribution, the systemic sensitivity to risk (henceforth sensitivity measure), and other "classic" network centrality measures such as the in/out-degree, and the hub-authorities. The table presents a ranking of the countries from "core" (1st to 5th), through "semi-periphery" (6th to 15th), to "periphery" (16th to 20th).

Rank	M^{sys}	S^{sys}	In-Deg	Out-Deg	Hub	Auth
			Core			
1	US – 0.443	US – 1.025	BE – 9	US – 16	US – 0.420	FR – 0.296
2	BR – 0.404	FR – 0.641	FR – 9	BR – 9	DE – 0.256	NL – 0.293
3	FR – 0.328	BR – 0.556	NL – 9	BE – 8	FR – 0.250	BE – 0.272
4	HK – 0.297	HK – 0.544	HK – 8	FR – 8	NL – 0.239	DE – 0.267
5	DE – 0.275	DE – 0.492	DE – 8	DE – 8	BE – 0.233	UK – 0.266
			Semi-Periphery			
6	IT – 0.251	NL – 0.459	IT – 8	NL – 8	IT – 0.215	CH – 0.257
7	ES – 0.250	ES – 0.457	ES – 8	CA – 7	CH – 0.215	IT – 0.253
8	NL – 0.217	CA – 0.435	CH – 8	HK – 7	UK – 0.212	ES – 0.247
9	RU – 0.205	IT – 0.430	UK – 8	IT – 7	BR – 0.204	HK – 0.206
10	JP – 0.202	MX – 0.427	AU – 7	ES – 7	ES – 0.204	JP – 0.206
11	KR – 0.201	BE – 0.405	JP – 7	CH – 7	CA – 0.173	PT – 0.204
12	MX – 0.198	KR – 0.394	KR – 7	UK – 7	KR – 0.155	RU – 0.191
13	BE – 0.164	UK – 0.347	PT – 7	MX – 6	HK – 0.149	AU – 0.190
14	CA – 0.150	JP – 0.345	RU – 7	JP – 6	MX – 0.147	KR – 0.188
15	UK – 0.146	RU – 0.310	BR – 6	KR – 6	PT – 0.140	US – 0.171
			Periphery			
16	IN – 0.138	AU – 0.295	US – 6	RU – 6	RU – 0.138	BR – 0.162
17	PT – 0.118	CH – 0.279	IN – 6	IN – 5	JP – 0.130	CA – 0.161
18	AU – 0.107	PT – 0.269	CA – 5	PT – 5	IN – 0.109	MX – 0.160
19	CH – 0.107	IN – 0.268	MX – 5	AU – 4	CN – 0.104	IN – 0.157
20	CN – 0.098	CN – 0.180	CN – 4	CN – 4	AU – 0.095	CN – 0.103

Table 7: Ranking of major stock markets into core, semi-periphery and periphery based on median summary statistics of network and local turbulence measures for full-sample.

The out-degree shows that the US (with 16 out-links) is by far the market with the highest influence on 16 out of 19 world markets. It is followed by Brazil with 9 out-links, and Belgium, France, and Germany tied with 8 out-links. The high ranking of the US as a hub for risk transmission is confirmed by the hub centrality. The relative importance of the hub centrality, however, ranks Germany above France, followed by the Netherlands and Belgium. Although

the core countries of the out-degree and hub centrality appear the same, the ranking is slightly different, except for the US as top-ranked according to both measures. The in-degree indicates a tie between Belgium, France, and the Netherlands, as the markets liable to be influenced by 9 other major markets. The authority centrality disentangled this tie by ranking France as the most influenced market, followed by the Netherlands and Belgium.

The marginal turbulence, (M^{sys}), ranks the country markets in terms of their "share" of the total turbulence, according to (25). The results in Table 7 show that the US has the highest contribution to financial market turbulence over the first two decades of the 21st century. It is closely followed by Brazil, France, Hong Kong, and Germany. China, on the other hand, contributes the lowest share of total turbulence. The sensitivity measure, S^{sys}, unlike the marginal turbulence, is a forward-looking measure of how much financial turbulence changes as a result of a change in the risk of a major world market index. The sensitivity result shows that the turbulence index is highly sensitive to the US market, more than any other. The second most relevant market is France, followed by Brazil, Hong Kong, and Germany. This suggests that a 100% shock to the US S&P 500 will increase financial turbulence by 102.5%, while the same 100% shock on France's CAC 40, Brazil's Bovespa, Hong Kong's Hang Seng and Germany's DAX 30 increases the turbulence by 64.1%, 55.6%, 54.4%, and 49.2%, respectively. The impact of the rest is much lower. In particular, the markets of China, India, Switzerland, and Australia (along with the Portuguese market) can be identified as peripheries, since shocks to them have less than 30% impact the global system.

Overall, the result shows that the US market is the most influential, and small changes in its risk causes the highest financial turbulence. In terms of turbulence contribution, the US is the first, followed by Brazil, France, Hong Kong, and Germany. The result also shows that, although Brazil has a higher contribution to turbulence than France, a small change in the risk of the French market have a higher turbulence amplification than that of Brazil.

5.3.2. Sub-Sample Systemic Relevance

We extend our response to RQ-3 by studying the relevance of the markets to financial turbulence over the four consecutive periods of five years, and 2020-Q1. Table 8 reports a ranking of the "core" (1st to 5th) countries in terms of median summary statistics of the marginal turbulence contribution, the systemic measure, and other "classic" network centrality measures such as the in/out-degree, and the hub-authorities.

2000-2004 is the early part of the 21st century, known to be characterized by the tech crisis, the September 11, and the stock market downturn of October 2002. The median summary statistics of Table 8 show that during this sub-period, the US market was the most influential (16 out of 19 out-links), and the hub for risk transmission. It was also the market with the highest contribution to turbulence, and whose change in risk significantly alters global market operations. During this period, the Netherlands was the most liable market to be influenced, and the highest receiver of risk.

2005–2009 coincides with the global financial crisis, triggered by endogenous shock events, fuelled by the sub-prime mortgages in 2007, the near-collapse and acquisition of Bear Sterns by JP Morgan Chase in March 2008, the bankruptcy of Lehman Brothers (4th-largest US investment bank at the time), and the bailout of American International Group (AIG, the world's largest insurance company) in September 2008. All these events began in the US. The summary statistics of Table 8 shows that for 2005–2009, the US market maintained its status as the most influential (17/19 out-links), and the hub for risk transmission. It was also the market with the highest contribution to turbulence, and whose change in risk significantly

Rank	M^{sys}	S^{sys}	In-Deg	Out-Deg	Hub	Auth
			2000 – 2004			
1	US – 0.764	US – 1.530	NL – 10	US – 16	US – 0.464	NL – 0.304
2	DE – 0.580	FR – 0.770	KR – 9	DE – 9	DE – 0.286	FR – 0.295
3	FR – 0.512	DE – 0.709	FR – 9	NL – 9	FR – 0.263	UK – 0.274
4	KR – 0.483	KR – 0.541	HK – 8	KR – 8	NL – 0.262	IT – 0.272
5	BR – 0.468	BR – 0.535	DE – 8	FR – 8	IT – 0.249	DE – 0.267
			2005 – 2009			
1	US – 0.556	US – 1.178	FR – 11	US – 17	US – 0.403	FR – 0.298
2	BR – 0.517	MX – 0.772	BE – 10	MX – 11	MX – 0.256	UK – 0.281
3	MX – 0.506	BR – 0.708	ES – 10	BR – 9	FR – 0.244	NL – 0.276
4	HK – 0.372	HK – 0.599	UK – 10	CA – 8	DE – 0.232	ES – 0.273
5	RU – 0.333	DE – 0.525	HK – 9	HK – 8	NL – 0.230	BE – 0.270
			2010 – 2014			
1	FR – 0.442	US – 0.873	BE – 10	US – 14	US – 0.368	FR – 0.296
2	BR – 0.425	FR – 0.731	FR – 10	BR – 13.5	BR – 0.365	NL – 0.286
3	IT – 0.370	BR – 0.697	DE – 9	BE – 8	DE – 0.245	BE – 0.283
4	US – 0.336	HK – 0.570	NL – 9	FR – 8	UK – 0.241	DE – 0.281
5	ES – 0.329	ES – 0.529	UK – 9	DE – 8	FR – 0.238	UK – 0.269
			2015 – 2019			
1	HK – 0.260	US – 0.829	BE – 9	US – 17	US – 0.466	NL – 0.310
2	US – 0.254	HK – 0.513	NL – 9	BE – 9	BE – 0.278	BE – 0.300
3	BR – 0.232	FR – 0.513	HK – 8	FR – 8	FR – 0.265	FR – 0.295
4	FR – 0.225	NL – 0.450	JP – 8	DE – 8	NL – 0.250	DE – 0.262
5	ES – 0.185	BE – 0.445	FR – 8	CH – 7.5	CH – 0.248	UK – 0.260
			2020:01 – 2020:03			
1	US – 1.393	US – 1.801	BE – 10	BE – 13	HK – 0.328	ES – 0.311
2	BE – 1.234	BE – 1.234	FR – 10	MX – 12	MX – 0.291	IT – 0.305
3	NL – 1.014	FR – 1.227	NL – 10	US – 12	NL – 0.288	NL – 0.305
4	FR – 0.969	NL – 1.187	IT – 9	HK – 12	IT – 0.283	BE – 0.299
5	BR – 0.719	HK – 0.923	PT – 9	IT – 11	FR – 0.276	FR – 0.297

Table 8: Core markets ranked according to network and local turbulence measures over sub-periods.

alters global market operations. During this period, France was the most liable market to be influenced, and the highest receiver of risk.

2010–2014 was characterized by the EU crisis which heavily affected EU markets. The results in Table 8 shows that the US market still maintained its status as the most influential (14/19 out-links) and the hub for risk transmission, as well as the market whose change in risk significantly changes financial turbulence. The difference, however, between this period and the preceding one is that France was the most liable market to be influenced and the highest receiver of risk, and the highest contributor to turbulence. This is not quite surprising since the European sovereign crisis mostly involved EU countries, as such the most contributor to global market disruption, will certainly be from the EU.

2015–2019 is highly characterized by the Chinese stock market turbulence and United Kingdom European Union membership referendum. The results in Table 8 shows that the US market still maintained its status as the most influential (17/19 out-links) and the hub for risk transmission, as well as the market whose change in risk profile significantly changes

financial market turbulence. The Netherlands was the most liable market to be influenced and the highest receiver of risk. The highest contributor to financial market turbulence during this period was Hong Kong. This is also not quite surprising since Hong Kong is the special administrative region of the People's Republic of China (HKSAR) and the Hang Seng index is often regarded as a reflection of China's economic rise.

The first quarter of 2020 (2020-Q1) is characterized by the COVID-19 crisis, triggered by an exogenous shock of non-financial origin affecting the real sector, first in China and then to the rest of the world. Unlike the previous crisis, the COVID-19 pandemic is characterized by high synchronicity between the markets (as depicted in Figure 5), with a fast spread of risks and uncertainty, not experienced before. Table 8 shows that, for the 2020-Q1, unlike any of the previous crises, the US market failed to maintain its status as the most influential and the hub for risk transmission. However, it is still the market with the highest contribution to turbulence, and whose change in risk profile significantly alter global market operations.

In summary, the evidence shows that during crises (periods with high magnitudes of financial turbulence, and severe disruptions on a much broader segment of financial markets), such as the tech (2000–2003), global financial crisis (2007–2009) and COVID-19 crisis (2020-Q1), the US plays a critical role as the highest contributor to turbulence. For the majority of these crises (except COVID-19, so far), the US is both the most influential and the hub for risk transmission. The results of the sensitivity of turbulence to individual risk remain the same over all the sub-periods. The consensus is that the US has the topmost market whose change in risk profile can significantly disrupt global market operations.

5.4. Robustness Checks

To validate our findings relating to RQ-2, we conduct further analysis by comparing our estimated risk effect indices with the Chicago Board of Exchange VIX index - a measure that reflects the market's expectation on the monthly volatility based on the S&P 500 index. Figure 6 plots the evolution of the two indices over our sample period. The figure shows a

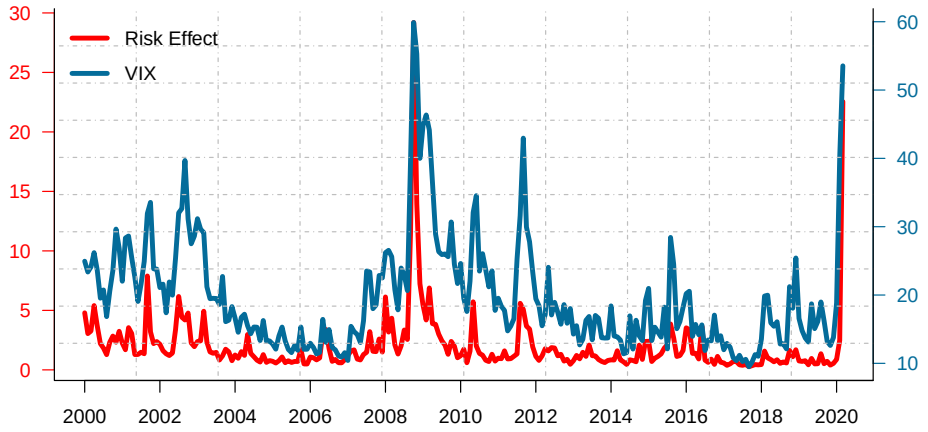

Figure 6: Comparing the VIX and Risk Effect.

high correlation between the two indices. Although VIX focuses on only one of our markets, and it is based on future expectations, rather than on past observations, the correlation with our risk effect estimates is 0.77. A similar correlation holds for the VIX with the turbulence index, as expected. The network density and the network effect indices, on the other hand, have lower correlations of 0.65 and 0.49, respectively. In terms of "peaks", the VIX reaches

the highest monthly averages in October 2008 and March 2020, in line with our results. The advantage of our proposed measure, compared to the VIX, is that it is based on multiple markets, rather than on a single one. Besides, our measure can disentangle the "individual" market volatility from that generated through interconnectedness.

6. Conclusion

In this paper, we construct a network-based turbulence score that proves useful for analyzing the relationship between financial interconnectedness, and global market risk, and for identifying systemically important markets, with the highest contribution to financial turbulence. We discussed three key features of our turbulence index: 1) The index scores the level of global market disruptions and signals the direction of financial markets with early warnings for investors; 2) The turbulence index decomposes into a product of two indicators, namely, risk and network effect. The risk effect records the magnitude of initial global market risk, and the network effect is the degree to which the interconnectedness among stock markets intensifies or weakens the initial global market risks; and 3) The index decomposes into marginal turbulence contribution and systemic sensitivity to individual risk, with both measures shown to be useful when assessing the relevance of a stock market to financial turbulence.

We apply our proposed measure to address three important questions in financial contagion analysis. The research questions are as follows: (RQ-1) Does a densely interconnected market reduce or amplify the financial risks caused by shock events? (RQ-2) Is there a threshold level of risk effect beyond which financial connection channels serve as shock-amplifiers? (RQ-3) Which major stock market is central to the creation of global financial turbulence?

We address the above questions by studying the integration among the major stock markets over the first two decades of the 21st century, particularly during the tech, sub-prime, and COVID-19 crises. The empirical result shows the following: 1) the correlation between network density and our turbulence index is about 0.556, which confirms the results of Billio et al. (2012) and Blume et al. (2013) that, densely interconnected markets amplify financial risks; 2) when risk effect (or global market risk) is above 2.0 of returns, and the network effect is beyond 3.9, global market conditions shift into a fragile state where financial connections serve as shock-amplifiers to cause turbulence; and 3) the US market is the most influential, and small changes in its risk causes the highest financial turbulence. For turbulence contribution, the US is ranked first, followed by Brazil, France, Hong Kong, and Germany. Although Brazil has a higher turbulence contribution than France, the turbulence index is more sensitive to a small change in the risk of the French market than that of Brazil.

We believe that our methodology can be quite useful, for policymakers, investors, and private individuals, as it provides results that are relatively easy to access and interpret, from a financial stability viewpoint.

Acknowledgements

The work in the paper has received support from the European Union's Horizon 2020 training and innovation program "FIN-TECH", under the grant agreement No. 825215 (Topic ICT-35-2018, Type of actions: CSA). The paper is the result of the collaboration between the two authors; however, Sections 1-4 and the Appendix have been written by DA, who has also written the software code; and Sections 5-6 by PG.

References

Acemoglu, D., A. Ozdaglar, and A. Tahbaz-Salehi (2015). Systemic Risk and Stability in Financial Networks. *American Economic Review 105*(2), 564–608.

Adrian, T. and M. K. Brunnermeier (2016). CoVaR. *The American Economic Review 106*(7), 1705–1741.

Ahelegbey, D. F., M. Billio, and R. Casarin (2016a). Bayesian Graphical Models for Structural Vector Autoregressive Processes. *Journal of Applied Econometrics 31*(2), 357–386.

Ahelegbey, D. F., M. Billio, and R. Casarin (2016b). Sparse Graphical Vector Autoregression: A Bayesian Approach. *Annals of Economics and Statistics 123/124*, 333–361.

Allen, F. and D. Gale (2000). Financial Contagion. *Journal of Political Economy 108*(1), 1–33.

Avdjiev, S., P. Giudici, and A. Spelta (2019). Measuring Contagion Risk In International Banking. *Journal of Financial Stability 42*, 36–51.

Banulescu, G.-D. and E.-I. Dumitrescu (2015). Which are the SIFIs? A Component Expected Shortfall Approach to Systemic Risk. *Journal of Banking and Finance 50*, 575–588.

Barigozzi, M. and C. Brownlees (2019). NETS: Network Estimation for Time Series. *Journal of Applied Econometrics 34*(3), 347–364.

Basu, S. and G. Michailidis (2015). Regularized Estimation in Sparse High-dimensional Time Series Models. *The Annals of Statistics 43*(4), 1535–1567.

Battiston, S., D. Delli Gatti, M. Gallegati, B. Greenwald, and J. E. Stiglitz (2012). Liaisons Dangereuses: Increasing Connectivity, Risk Sharing, and Systemic Risk. *Journal of Economic Dynamics and Control 36*(8), 1121–1141.

Billio, M., M. Getmansky, A. W. Lo, and L. Pelizzon (2012). Econometric Measures of Connectedness and Systemic Risk in the Finance and Insurance Sectors. *Journal of Financial Economics 104*(3), 535 – 559.

Blume, L., D. Easley, J. Kleinberg, R. Kleinberg, and É. Tardos (2013). Network Formation in the Presence of Contagious Risk. *ACM Transactions on Economics and Computation 1*(2), 6.

Bonacich, P. (1972). Technique for Analyzing Overlapping Memberships. *Sociological Methodology 4*, 176–185.

Borgatti, S. P. and M. G. Everett (2006). A Graph-Theoretic Perspective on Centrality. *Social Networks 28*(4), 466–484.

Brownlees, C. and R. F. Engle (2017). SRISK: A Conditional Capital Shortfall Measure of Systemic Risk. *The Review of Financial Studies 30*(1), 48–79.

Carvalho, C., H. Massam, and M. West (2007). Simulation of Hyper-inverse Wishart Distributions in Graphical Models. *Biometrika 94*, 647–659.

Carvalho, C. M. and M. West (2007). Dynamic Matrix-Variate Graphical Models. *Bayesian Analysis 2*, 69–98.

Casella, G. and C. P. Robert (2004). *Monte Carlo Statistical Methods*. New York: Springer Verlag.

Corander, J. and M. Villani (2006). A Bayesian Approach to Modelling Graphical Vector Autoregressions. *Journal of Time Series Analysis 27*(1), 141–156.

Dawid, A. P. and S. L. Lauritzen (1993). Hyper Markov Laws in the Statistical Analysis of Decomposable Graphical Models. *The Annals of Statistics 21*(3), 1272–1317.

Diebold, F. and K. Yilmaz (2014). On the Network Topology of Variance Decompositions: Measuring the Connectedness of Financial Firms. *Journal of Econometrics 182*(1), 119–134.

Faust, K. (1997). Centrality in Affiliation Networks. *Social Networks 19*(2), 157–191.

Freeman, L. C. (1978). Centrality in Social Networks Conceptual Clarification. *Social Networks 1*(3), 215–239.

Freixas, X., B. M. Parigi, and J.-C. Rochet (2000). Systemic Risk, Interbank Relations, and Liquidity Provision by the Central Bank. *Journal of Money, Credit and Banking 32*(3), 611–638.

Geiger, D. and D. Heckerman (2002). Parameter Priors for Directed Acyclic Graphical Models and the Characterization of Several Probability Distributions. *Annals of Statistics 30*(5), 1412–1440.

Gelman, A. and D. B. Rubin (1992). Inference from Iterative Simulation Using Multiple Sequences, (with discussion). *Statistical Science 7*, 457–511.

George, E. I., D. Sun, and S. Ni (2008). Bayesian stochastic search for VAR model restrictions. *Journal of Econometrics 142*, 553–580.

Giudici, P. and P. J. Green (1999). Decomposable Graphical Gaussian Model Determination. *Biometrika 86*(4), 785–801.

Giudici, P. and A. Spelta (2016). Graphical Network Models for International Financial Flows. *Journal of Business & Economic Statistics 34*(1), 128–138.

Grzegorczyk, M. and D. Husmeier (2008). Improving the Structure MCMC Sampler for Bayesian Networks by Introducing a New Edge Reversal Move. *Journal of Machine Learning 71*(2), 265–305.

Haldane, A. G. (2013). Rethinking The Financial Network. In *Fragile stabilität–stabile fragilität*, pp. 243–278. Springer.

Härdle, W. K., W. Wang, and L. Yu (2016). TENET: Tail-Event driven NETwork risk. *Journal of Econometrics 192*(2), 499–513.
Hoff, P. D. (2008). Modeling Homophily and Stochastic Equivalence in Symmetric Relational Data. In *Advances in Neural Information Processing Systems*, pp. 657–664.
Huang, X., H. Zhou, and H. Zhu (2012). Systemic Risk Contributions. *Journal of Financial Services Research 42*(1-2), 55–83.
Kinlaw, W. and D. Turkington (2013). Correlation Surprise. *Journal of Asset Management 14*(6), 385–399.
Kritzman, M. and Y. Li (2010). Skulls, Financial Turbulence, and Risk Management. *Financial Analysts Journal 66*(5), 30–41.
Kritzman, M., Y. Li, S. Page, and R. Rigobon (2011). Principal Components as a Measure of Systemic Risk. *Journal of Portfolio Management 37*(4), 112.
Li, Y., S. Zhu, D. Li, and D. Li (2013). Active Allocation of Systematic Risk and Control of Risk Sensitivity in Portfolio Optimization. *European Journal of Operational Research 228*(3), 556–570.
Newman, M. (2010). *Networks: An Introduction.* Oxford University Press.

Appendix A. Sampling Algorithms

The algorithm for sampling $G_{1:p}$ and G_0 is a modified version of the collapsed Gibbs scheme of Ahelegbey et al. (2016a). The first step of each Gibbs sampler is as follows:

1. Sample $[G_{1:p}|\mathcal{D}]$
2. Sample $[G_0|\mathcal{D}, G_{1:p}]$

Appendix A.1. Sampling Lag Network

1. Initialization for sampling $G_{1:p}$
   (a) Compute the reference score for each dependent node Y_i by $P(Y_i|\mathcal{D})$
   (b) Compute the score for each node $Z_j \in Z$ as a predictor of Y_i by $P(Y_i|Z_j, \mathcal{D})$
   (c) Compute the Bayes Factor $BF_{ij|1:p} = \log P(Y_i|Z_j, \mathcal{D}) - \log P(Y_i|\mathcal{D})$
   (d) Convert Bayes Factor per node score to adjacency matrix, $G_{ij|1:p} = 1$ if $BF_{ij|1:p} > 0$

2. Start MCMC such that at each iteration:
   (a) Let $Z_c \in Z$ denote the current set of predictors of Y_i, i.e., $G_{ic|1:p} = 1$
   (b) Randomly draw $Z_r \sim \{Z_1, \ldots, Z_{np}\}$ and update Z_c such that

$$Z_k = \begin{cases} (Z_c \cup Z_r) & \text{if } Z_r \notin Z_c \\ (Z_c \backslash Z_r) & \text{if } Z_r \in Z_c \end{cases}$$

   (c) Compute the old score $= P(Y_i|Z_c, \mathcal{D})$, and new score $= P(Y_i|Z_k, \mathcal{D})$ and

$$\phi = \frac{P(Y_i|Z_k, \mathcal{D})}{P(Y_i|Z_c, \mathcal{D})}$$

   (d) Sample $u \sim \mathcal{U}[0, 1]$ from a uniform distribution. If $u < \min\{1, \phi\}$, update $Z_c = Z_k$, otherwise leave it unchanged. Note that if $P(Y_i|Z_k, \mathcal{D}) > P(Y_i|Z_c, \mathcal{D})$, then the set of indexes in Z_k are better predictors of Y_i than Z_c and $G_{ik|1:p} = 1$.

Appendix A.2. Sampling Contemporaneous Network

1. Initialization for sampling G_0
   (a) Compute the reference score for each dependent node $Y_i|W_z$ by $P(Y_i|W_z, \mathcal{D})$
   (b) Compute the score for each node $Y_j \in Y_{-i}$ as a predictor of Y_i by $P(Y_i|Y_j, W_z, \mathcal{D})$
   (c) Compute the Bayes Factor, $BF_{ij|0} = \log P(Y_i|Y_j, W_z, \mathcal{D}) - \log P(Y_i|W_z, \mathcal{D})$

(d) Convert Bayes Factor per node score to adjacency matrix, $G_{ij|0} = 1$ if $BF_{ij|0} > 0$

2. Start MCMC such that at each iteration:
   (a) Let $Y_c \in Y_{-i}$ denote the current set of predictors of Y_i, i.e., $G_{ic|0} = 1$
   (b) Randomly draw $Y_r \sim \{Y_1, \ldots, Y_n\} \backslash \{Y_i\}$ and update Y_c such that

$$Y_k = \begin{cases} (Y_c \cup Y_r) & \text{if } Y_r \notin Y_c \\ (Y_c \backslash Y_r) & \text{if } Y_r \in Y_c \end{cases}$$

   (c) Compute the old score $= P(Y_i|Y_c, W_z, \mathcal{D})$, and new score $= P(Y_i|Y_k, W_z, \mathcal{D})$ and

$$\phi = \frac{P(Y_i|Y_k, W_z, \mathcal{D})}{P(Y_i|Y_c, W_z, \mathcal{D})}$$

   (d) Sample $u \sim \mathcal{U}[0, 1]$ from a uniform distribution. If $u < \min\{1, \phi\}$, update $Y_c = Y_k$, otherwise leave it unchanged. Note that if $P(Y_i|Y_k, W_z, \mathcal{D}) > P(Y_i|Y_c, W_z, \mathcal{D})$, then the set of indexes in Y_k are better predictors of Y_i than Y_c and $G_{ik|0} = 1$.